

MODELLING BIFACIAL PHOTOVOLTAIC SYSTEMS

Evaluating the albedo impact on bifacial PV systems based on case studies in Denver, USA and Västerås, Sweden

ANTON NYGREN

ELIN SUNDSTRÖM

School of Business, Society and Engineering
Course: Degree Project in Energy Engineering
Course code: ERA402
Credits: 30 hp
Program: M.Sc. in Industrial Engineering and Management

Supervisor: Bengt Stridh
Examinor: Hailong Li
Costumer: Mälardalen University
Date: 2021-06-11
Email:
ann16019@student.mdh.se
esm15004@student.mdh.se

ABSTRACT

This study aims to develop a simulation and optimisation tool for bifacial photovoltaic (PV) modules based on the open-source code OptiCE and evaluate dynamic and static albedo impact on a bifacial PV system. Further, a review of the market price development of bifacial PVs' and an optimisation to maximise energy output was conducted. Two case studies with bifacial PV modules, a single-axis tracker in Denver, USA, and a vertical and a tilted system installed at a farm outside Västerås, Sweden, were analysed in this study. The results showed that an hourly dynamic albedo value could provide more accurate simulation results of the rear side irradiance for the bifacial single-axis tracker than a static albedo value. The developed model showed an R² accuracy of 93% and 91% for the front and rear sides, respectively, when simulated with an hourly albedo value for the bifacial single-axis tracker system. The optimisation was based on weather data from 2020. The results showed that the tilted reference system could increase its energy output by 8.5% by adjusting its tilt from 30° to 54° and its azimuth angle from 0 to -39°. In contrast, the vertical system would increase its energy output by 2.1% by rotating the azimuth angle from -90° to -66°. Conclusions that could be drawn are that bifacial PV price has closed in on the high-performance monofacial PV price the last five years and may continue to decrease in the coming years. Further, it was concluded that detailed dynamic albedo values lead to more accurate simulations of the ground-reflected irradiance. The availability of measured albedo data at the location is essential when the ground-reflected irradiance stands for a significant share of the irradiance. It was determined that during 2020 the optimal configurations of a vertical and tilted bifacial PV system in Västerås would save 11 300 SEK by consuming self-produced electricity and earn 11 600 SEK from selling the surplus of electricity for the farm outside Västerås.

Keywords: Bifacial PV, albedo, modelling photovoltaics, solar radiation, module price, OptiCE

PREFACE

This study is a degree project in Energy Engineering at Mälardalen University in Västerås, Sweden, written by Anton Nygren and Elin Sundström during the spring semester of 2021. The study has been conducted in cooperation with the research project *Evaluation of the first agrivoltaic system in Sweden*, at Mälardalen University, with Dr Pietro Elia Campana and Dr Bengt Stridh. We want to thank both Pietro Campana and Bengt Stridh for their guidance and support throughout the project. Your insightful feedback has helped us improve our work.

Further, we would like to thank our examiner Hailong Li for his valuable suggestions and comments during the progress of our thesis. We also want to acknowledge and thank Dr Bill Marion, Dr Silvana Ayala Pelaez, Dr Chris Deline, and the National Renewable Energy Laboratory for providing data in the data hub DuraMAT. Finally, we thank our classmates that have provided us with insightful opposition during this spring.

Västerås in June 2021



Anton Nygren



Elin Sundström



MÄLARDALEN UNIVERSITY
SWEDEN

SUMMARY

Solar photovoltaics have increasingly become a vital renewable energy source globally. New technical innovations such as bifacial PV modules show good energy return also using the rear side of the module to receive irradiance. Previous research has identified the difficulties in simulating the energy generation from the rear side due to illumination variation. The rear side of tilted bifacial PV modules is dependent on the ground-reflected irradiance. The dependency enforces the importance of simulation with a precise value of the ground surface reflectivity, also called albedo. This study aimed to develop a model to simulate the performance of bifacial PV modules and assess the impact of the grounds' albedo value. Also, the study aimed to evaluate which tilt and azimuth angle maximises the energy output of two bifacial PV systems in Västerås, Sweden.

A literature study was made to research the market price development of bifacial PV technologies and previous studies within bifacial PV. The literature study contributed to the mathematical framework for the developed model by exploring equations from scientific research and the open-source library PVLIB ToolBox. The developed model was based on the open-source model OptiCE in Matlab. The optimisation was achieved with the built-in genetic algorithm in OptiCE. Two case studies were used during this study: a bifacial single-axis tracker system in Denver, USA, and two recently installed bifacial PV systems (one tilted and one vertical) at a farm in Västerås, Sweden. Only measurements for the system in Denver was available, which limited the validation of the developed model to the single-axis tracker system.

The main result of this study shows that a mathematical model for bifacial PV modules has been developed that can simulate both the received front and rear irradiance and energy output. The model was validated to measurements of front and rear irradiance for the bifacial single-axis tracker system. The R² accuracy of the model with hourly albedo was 93% and 91% for the front and rear side, respectively. PVsyst simulations with a fixed albedo showed similar precision for the front side (94%) and lower accuracy for the rear side (42%). The rear side irradiance simulations with a satellite-derived albedo value and a fixed albedo value resulted in a lower accuracy than the hourly albedo value. In contrast, the front side showed similar accuracy for all three albedo alternatives. The result was caused by the rear side receiving a significant share of ground-reflected irradiance. However, advanced measurement equipment is required to calculate hourly albedo values. The optimisation result showed that the tilted reference and vertical PV systems' energy generation could increase by 8.5% and 2.1%, respectively, compared to the installed configurations. The literature study showed how the price of bifacial PV modules had decreased over the last five years, thus increasing the competitiveness against monofacial PV modules.

The conclusion was drawn that when the ground-reflected irradiance is a large share of the irradiance, a dynamic albedo value is necessary to achieve an accurate simulation result. With optimal angles would the farm in Västerås, Sweden, save 11 300 SEK from self-consuming produced electricity and earn 11 600 SEK in selling electricity 2020 (total capacity of 34.64 kW). However, the optimisation result should be regarded cautiously since the developed model is not validated against the systems at the farm.

SAMMANFATTNING

Solceller har alltmer blivit en väsentlig global förnybar energikälla. Nya tekniska innovationer som tvåsidiga solcellsmoduler påvisar god energiavkastning till följd av baksidans förmåga att ta emot solinstrålning. Tidigare studier har identifierat svårigheter inom simulering av energigeneration från baksidan på grund av ljusvariationer. Baksidan på tvåsidiga solcellsmoduler är beroende av markreflekterad Detta stärker vikten av simuleringar med korrekt värde på markens reflexionsförmåga, även kallad albedo. Syftet med denna studie var att utveckla en modell för att simulera tvåsidiga solcellsmoduler och utvärdera effekten av markens albedo. Samt var syftet att utvärdera vilka lutnings- och orienterings vinklar som maximera elproduktionen för två tvåsidiga solpanelssystem i Västerås, Sverige.

En litteraturstudie genomfördes för att utforska marknadsprisutvecklingen för tvåsidiga solcellsteknologier och tidigare studier inom tvåsidiga solcellsmoduler. Litteraturstudien bidrog till det matematiska ramverket för den utvecklade modellen genom att använda ekvationer från vetenskaplig forskning och öppna källbiblioteket PVLIB ToolBox. Den utvecklade modellen var baserad på den öppna källkoden OptiCE i Matlab. Optimeringen uppnåddes genom en inbyggd genetisk algoritm i OptiCE. Två fallstudier användes i denna studie: ett tvåsidigt 1-axlig solföljningssystem i Denver, USA, och två fast installerade tvåsidiga solpanelssystem (ett lutat och ett vertikalt) på en gård i Västerås, Sverige. Endast driftdata för systemet i Denver var tillgängligt, vilket begränsade valideringen av den utvecklade modellen till 1-axliga solföljningssystemet.

Det huvudsakliga resultatet av denna studie är att en matematisk modell för tvåsidiga solcellsmoduler har utvecklats som kan simulera både framsidan och baksidans mottagna instrålning och elproduktion. Modellen validerades mot mätningar av fram- och bakinstrålning för det tvåsidiga 1-axliga solföljningssystemet. R² precisionen för modellen med tim-albedo var 93% för framsidan och 91% för baksidan. PVsyst simuleringar med ett konstant albedovärde visade liknande precision för framsidan (94%) och lägre precision för baksidan (42%). Simulering av baksidans instrålning med satellit-hämtade albedovärden och konstant albedovärde resulterade i lägre exakthet än med tim-albedovärden. I motsats till, visade framsidan liknande exakthet för alla tre alternativ. Resultatet beror av att baksidan mottar en signifikant andel markreflekterad instrålning. Däremot, avancerad mätutrustning är nödvändig för att beräkna tim-albedovärden. Optimeringsresultatet visade att det lutade och vertikala PV systemens elproduktion kunde öka med 8,5% respektive 2,1% jämfört med de installerade konfigurationerna. Litteraturstudien visade att priset för tvåsidiga solcellsmoduler har minskat under de senaste fem åren, således ökar konkurrenskraften mot ensidiga solcellsmoduler.

Slutsatsen drogs att när markreflekterad instrålning är en stor del av instrålningen är ett dynamiskt albedovärde väsentligt för att åstadkomma tillförlitliga simuleringsresultat. Med optimala vinklar skulle gården i Västerås, Sverige, spara 11 300 SEK i att konsumera egenproducerad elektricitet och tjäna 11 600 SEK i att sälja överskottselektricitet (total kapacitet på 34.64 kW). Optimeringsresultatet borde dock beaktas varsamt eftersom den utvecklade modellen inte är validerad mot systemen på gården.

CONTENT

- 1 INTRODUCTION1**
 - 1.1 Background 1**
 - 1.2 Problem definition 3**
 - 1.3 Purpose..... 3**
 - 1.4 Research questions 3**
 - 1.5 Scope and delimitations 4**

- 2 METHOD5**
 - 2.1 Literature study 5**
 - 2.2 Developing and validating the model..... 5**
 - 2.3 Evaluation of the impact of albedo value..... 7**
 - 2.4 Find and evaluate optimal configurations for Kärrobo Prästgård..... 7**

- 3 LITERATURE STUDY9**
 - 3.1 PV technologies..... 9**
 - 3.1.1 Bifacial PV 9*
 - 3.1.2 Cell technologies..... 10*
 - 3.1.3 PV system performance metrics 11*
 - 3.2 Market price development12**
 - 3.3 The albedo value14**
 - 3.3.1 The impact on ground-reflected irradiance 14*
 - 3.3.2 Albedo measurements 15*
 - 3.3.3 Albedo modelling 15*
 - 3.4 System configurations & surrounding factors17**
 - 3.5 OptiCE and genetic algorithms in previous research18**

- 4 MODEL AND CASE STUDIES20**
 - 4.1 Model framework.....20**
 - 4.2 Front and Rear Irradiance21**
 - 4.2.1 Solar and PV module angles and directions.....21*

4.2.2	<i>Reflection losses</i>	22
4.2.3	<i>Direct beam irradiance</i>	23
4.2.4	<i>Diffuse irradiance</i>	23
4.2.5	<i>Ground-reflected irradiance</i>	25
4.3	Power generation	29
4.4	NREL BEST field	30
4.4.1	<i>Hourly, satellite-derived and fixed albedo</i>	31
4.5	Kärrobo Prästgård	32
4.5.1	<i>Hourly and fixed albedo</i>	33
4.5.2	<i>Optimisation of system configurations</i>	34
4.5.3	<i>Value of electricity</i>	35
5	RESULTS	38
5.1	Validation of the model: NREL BEST-field	38
5.2	Albedo effect on the irradiance: NREL BEST-field	41
5.3	Optimisation results: Kärrobo Prästgård	43
6	DISCUSSION	46
6.1	Market price development of bifacial PV	46
6.2	Validation of model and evaluation of albedo	46
6.3	Optimal configurations of Kärrobo Prästgård	48
7	CONCLUSION	51
8	FURTHER STUDIES	52
9	REFERENCES	53

LIST OF FIGURES

Figure 1	Radiation on a bifacial PV module.....	2
Figure 2	Schematic flow chart of the methodology.....	5
Figure 3	Schematic drawing of an industry-typical monofacial PERC cell and a bifacial PERC+ cell.....	9
Figure 4	Schematic drawings of the bifacial PERC+ cell in bifacial glass-glass PV modules and monofacial PV modules with a white back sheet	10
Figure 5	Cost gap between bifacial and conventional modules	13
Figure 6	EU spot market module prices by technology	13
Figure 7	Cost model results for cell conversion and module assembly	14
Figure 8	Overall model framework.....	20
Figure 9	Solar irradiance components	21
Figure 10	Angles of PV module	22
Figure 11	Self-shading of ground-reflected light from isotropic light.	26
Figure 12	Self-shading of ground-reflected light from direct (Dir) and circumsolar diffuse light ($Diff_{cir}$) (own illustration, inspiration from Sun et al. (2018)).....	27
Figure 13	Illustration of view factor of the shaded ground to the rear side of the module....	28
Figure 14	Matlab code for calculating the view factor	29
Figure 15	Picture of the bifacial PV modules installed at NREL BEST-field.....	30
Figure 16	Albedo alternatives for seven months in 2019-2020 at NREL BEST-field.....	31
Figure 17	Albedo alternatives from the 10 th to the 15 th of November 2019 at NREL BEST-field.	32
Figure 18	Picture of the vertical system & reference system installed at Kärrobo Prästgård...	32
Figure 19	Hourly albedo from Roskilde and fixed albedo from Kärrobo Prästgård, for 2020.	33
Figure 20	Hourly albedo from Roskilde and fixed albedo from Kärrobo Prästgård, for five days in June 2020.	34
Figure 21	Graph of the electric hourly load curve for Kärrobo Prästgård, the year 2020.	35
Figure 22	Monthly average spot price of electricity, the year 2020	36
Figure 23	Calculated value of electricity for bought and sold electricity 2020.....	37

Figure 24	Scatterplots of front and rear irradiance with the developed model (hourly albedo and fixed albedo) and PVsyst (fixed albedo) - NREL BEST field, for Oct-Apr	39
Figure 25	Irradiance components on the front and rear side of the results from the developed model with hourly and fixed albedo and PVsyst compared to the measured irradiance– NREL BEST field, for Oct-Apr	40
Figure 26	Scatterplots of the simulated result of front and rear irradiance with hourly, fixed and satellite-derived albedo - NREL BEST field, for Oct-Nov & Apr-Mar	41
Figure 27	Scatterplots of the simulated result of rear irradiance with a fixed albedo of 0.15, 0.30, 0.45 and 0.60 - NREL BEST field, for Oct-Nov & Apr-Mar	42
Figure 28	Irradiance components on the front and rear side of the vertical system with hourly and fixed albedo for optimal and installed configurations – Kärrobo Prästgård, 2020.....	44
Figure 29	Irradiance components on the front and rear side of the reference system with hourly and fixed albedo for optimal and installed configurations – Kärrobo Prästgård, 2020.....	45

LIST OF TABLES

Table 1	Surface albedos	2
Table 2	Performance metrics.	7
Table 3	Efficiency and bifaciality factor of c-Si cell technologies.	10
Table 4	Brightness Coefficients.....	25
Table 5	PV system characteristics of BEST field.....	31
Table 6	Characteristics of the installed systems at Kärrobo Prästgård.	33
Table 7	Boundaries of system configurations for optimisation.	34
Table 8	Price of components.....	36
Table 9	Comparison of performance metrics from the developed model (hourly and fixed albedo) and PVsyst (fixed albedo) – NREL BEST field, for Oct-Apr.....	40
Table 10	Comparison of performance metrics for hourly, fixed and satellite-derived albedo – NREL BEST field, Oct-Nov & Apr-Mar.	42

Table 11 Comparison of performance metrics for a fixed albedo of 0.15, 0.30, 0.45 and 0.6 – NREL BEST field, Oct-Nov & Apr-Mar..... 43

Table 12 Result of the optimisation and the installed configurations with fixed albedo (0.2) for 2020..... 43

Table 13 Result of the optimisation and the installed configurations with hourly albedo for 2020. 44

NOMENCLATURE

Symbol	Description	Unit
a_r	Angular loss coefficient	-
BF	Bifaciality factor	%
c_1	Fitting parameter	-
c_2	Fitting parameter	-
C	Constant depending on the surface type	-
d	Day of the year	-
E	Module elevation	m
F_1	Circumsolar brightness coefficient	-
F_2	Horizon brightness coefficient	-
f	Fraction	-
f_{ij}	Brightness coefficient	-
H	Module height	m
I	Diffuse horizontal irradiance	W/m^2
I_0	Diode reverse saturation current	A
I_C	Current	A
I_L	light current	A
k	Boltzmann's constant	J/K
L_s	Shadow length	m
m	Air mass	-
N_s	Number of cells in series	-
n	Ideality factor	-
f_{diff}	Diffuse fraction	-
P	Power	W
P_{mp}	Maximum power	W
q	Electronic charge	coulomb
R_{loss}	Reflection loss	-
R_S	Series resistance	Ohm
R_{Sh}	Shunt resistance	Ohm
SC	Solar constant	W/m^2
T	Temperature	K, °C
VF	View factor	-
VSA	Vertical shadow angle	°
x	Ground position	m

Symbol	Description	Unit
α_s	Solar altitude angle	°
β	Surface tilt angle	°
γ	Surface azimuth angle (0°=south, 180°=north)	°
γ_s	Solar azimuth angle (0°=south, 180°=north)	°
Δ	Brightness parameter	-
ε	Clearness parameter	-
η_c	Module Efficiency	-
θ	Angle of incidence	°
θ_M	Masking angle	°
θ_z	Zenith angle	°
ρ	Ground albedo	-
Ω_i	Solar geometry	°

INDEX

Index	Description
<i>alb</i>	Albedo / Ground-reflected
<i>beam</i>	Beam
<i>bs</i>	Black sky
<i>cir</i>	Circumsolar
<i>DHI</i>	Diffuse horizontal irradiance
<i>dir</i>	Direct
<i>diff</i>	Diffuse
<i>DNI</i>	Direct normal irradiance
<i>Extra</i>	Extra-terrestrial normal-incidence irradiance
<i>F</i>	Front
<i>GHI</i>	Global horizontal irradiance
<i>grd</i>	Ground
<i>hor</i>	Horizon
<i>iso</i>	Isotropic
<i>ns</i>	Not shaded
<i>R</i>	Rear

Index	Description
<i>tot</i>	Total
<i>ws</i>	White sky

ABBREVIATIONS

Abbreviation	Description
BEST	Bifacial Experimental Single-Axis Tracker
c-Si	Crystalline Silicon
DSO	Distribution System Operator
GA	Genetic Algorithm
HLT	Hight Load Time
IBC	Interdigitated Back Contact
IC	Installed Configurations
LCOE	Levelized Cost Of Electricity
LLT	Low Load Time
MAE	Mean Average Error
MBE	Mean Bias Error
NOCT	Nominal Operating Cell Temperature
NREL	National Renewable Energy Laboratory
OPT	Optimal Configurations
PERC	Passivated Emitter Rear Contact
PERL	Passivated Emitter Rear Locally Diffused
PERT	Passivated Emitter Rear Totally Diffused
PM	Performance metric
PV	Photovoltaics
R^2	Coefficient of Determination
RMSE	Root Mean Square Error
RS	Reference System
SEK	Swedish Krona
SHJ	Silicon Hetero-Junction
SMHI	Swedish Meteorological and Hydrological Institute
STC	Standard Test Condition

Abbreviation	Description
USD	US Dollar
VS	Vertical System

DEFINITIONS

Definition	Description
Albedo	The fraction of sunlight that a surface reflects
Bifacial module	PV module that absorbs light from the front and rear surface
Bifacial gain	Additional rear-side yield compared to the front side
Bifaciality	The ratio of the rear side efficiency to the front side efficiency
Monofacial module	PV module that absorbs light from the front
Specific yield	The ratio between total annual energy produced and the solar installed capacity

1 INTRODUCTION

Solar photovoltaics (PV) has become one of the fastest-growing renewable energy sources in the world. The global power generation from solar PV reached 720 TWh in 2019 and became the third-largest renewable electricity technology after hydropower and onshore wind (IEA, 2019). Improving the efficiency and cost-effectivity of PV technologies are a continuous process supported by material cost reductions and government support (Tyagi, Rahim, Rahim, & Selvaraj, 2013). Bifacial PV modules were developed to increase the power output compared to conventional monofacial PV modules since bifacial PV modules can absorb solar radiation from both the front and rear side (Cuevas, Luque, Eguren, & del Alamo, 1982). In this study, bifacial PV modules are mathematically modelled using Matlab. The developed model is based on OptiCE (n.d.) and will be used for simulations and optimisations of two bifacial PV systems.

1.1 Background

In 2020, the world market share for PV modules was dominated by monofacial modules (Fischer, Woodhouse, Herritsch, & Trube, 2021). At the same time, bifacial PV modules stood for 17% of the market share. Recent competitive projects have increased the market confidence in bifacial PV performance (Masson & Kaizuka, 2020). By assuming that bifacial and monofacial module have similar costs, Patel, Khan, Sun and Alam (2019) found a reduction of LCOE by about 2-6% for bifacial over monofacial PV module farms at latitudes higher than 30°. Khan, Hanna, Sun and Alam (2017) add that the energy gain must be carefully balanced with the increased installation cost to ensure the investment's economic viability for a bifacial PV system. Despite higher overall installation costs, bifacial PVs' performance shows competitiveness in the market (Masson & Kaizuka, 2020). The International Technology Roadmap for Photovoltaic predicts that the market share for bifacial PV modules will increase in the coming years and go beyond 55% in 2031 (Fischer et al., 2021).

One crucial obstacle for bifacial technology is to be considered bankable¹ to increase its market share. Therefore, predicting the energy yield of a bifacial PV system and comparing it to a conventional system is essential. The energy yield of a bifacial PV module compared to the energy yield of a monofacial PV module is known as the bifacial gain (Shoukry, Libal, Kopecek, Wefringhaus, & Werner, 2016). The bifacial gain of a bifacial PV module is affected by prerequisites involving the location and deployment (Rodríguez-Gallegos et al., 2018). Katsaounis et al. (2019) state that a bifacial PV system's deployment faces several challenges

¹ Likely to attract investment or considered stable enough to ensure profitability (Collins, 2021)

today than the conventional monofacial system. The main reason for these challenges is evaluating the field performance due to illumination variations on the rear surface.

Different authors mention several parameters that aggravate the simulation of the rear surface. Both Wang et al. (2015a) and Sun, Khan, Deline and Alam (2018) state that the essential parameters are diffused radiation, ground reflectance, module elevation, orientation, and tilt angle. The direct, diffuse and ground-reflected radiation on a bifacial PV module is illustrated in Figure 1, where E and H are the PV module's elevation and height. The albedo, or ground reflectance, is a unitless quantity that specifies the fraction of the incident sunlight that the surface reflects (National Snow & Ice Data Center, 2020). The scale varies between 0 and 1, with 0 meaning a perfect absorber and that no solar energy is reflected.

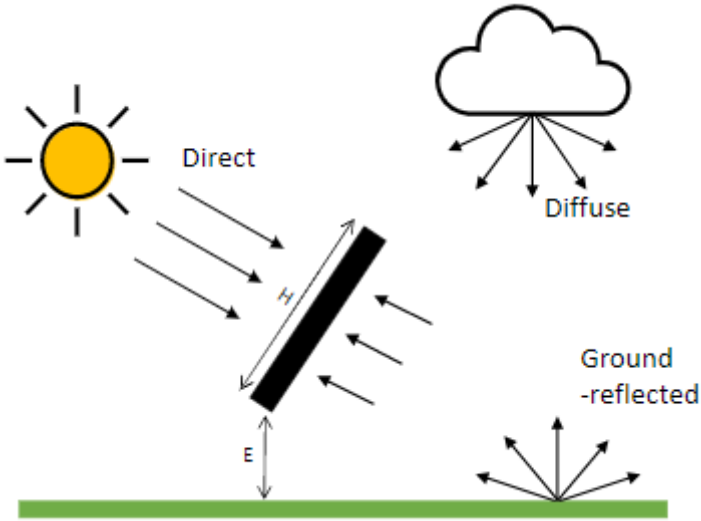


Figure 1 Radiation on a bifacial PV module (own illustration, inspiration from Sun et al. (2018)).

The albedo value is not strictly a fixed property of a surface since the reflected fraction depends on the angular and spectral effect (Iqbal, 1983). It includes sun position, solar spectrum, diffuse and beam irradiation, season and latitude. Chiodetti et al. (2016) state that daily albedo variations can reach up to 60 % for grass between morning and noon due to the incident angle of the light. Water can also achieve much higher reflectivity depending on the angle of incidence (Shaw & Vollmer, 2017). The albedo value is also affected by what kind of surface type is present at the location and if the surface is wet or not (Hutchins, 2020a; Iqbal, 1983). Some typical values are presented in Table 1.

Table 1 Surface albedos (data taken from Climatedata (n.d.) and Iqbal (1983)).

Surface type	Range of albedo
Snow	0.4 - 0.9
Sand	0.4
Grassland	0.15 - 0.25
Deciduous trees	0.15 - 0.18
Coniferous forest	0.08 - 0.15
Ocean	0.07 - 0.1

1.2 Problem definition

Bifacial PV module technology has shown promising results in energy yield compared to conventional monofacial PV modules. Calculating the energy production gain is essential for evaluating a bifacial PV systems' profitability (Shoukry et al., 2016). However, bifacial modules have proven to be more complex in simulations due to illumination variations on the rear surface (Stein et al., 2021). Compared to monofacial PV modules, the rear side of bifacial PV modules is more dependent on ground-reflected light (Lindsay et al., 2015). Several software tools have been developed to evaluate bifacial PV performance. PVsyst is one of these tools (PVsyst, n.d.a). However, PVsyst does not recommend simulating with tilt angles over 60 degrees, and the albedo values can only be adjusted at the highest frequency each month (Mermoud & Wittmer, 2016; PVsyst, n.d.b). Chiodetti et al. (2016) point out that considering a constant albedo is not sufficient when simulating some PV applications, for example, the yield of bifacial PV modules. OptiCE software is an open-source code with a PV simulation tool. OptiCE provides flexibility for the user but does not include bifacial PV modules as a simulation option (OptiCE, n.d.). As the bifacial PV technique increases in popularity, it becomes necessary to evaluate how surrounding factors and system configurations, such as albedo value, tilt angle and azimuth angle, influence power output. Various researches have investigated how different fixed albedo affect the energy yield of monofacial or bifacial PV systems (Sreenath, Sudhakar, & Yusop, 2021; Lindsay et al., 2015; Asgharzadeh et al., 2018). However, there is a lack of sufficient research on the impact on the power output when simulating with a dynamic albedo compared to a static albedo value.

1.3 Purpose

This study aims to develop the OptiCE model to simulate the performance of bifacial PV modules and evaluate the effect of the albedo value. Also, the aim is to assess what system configurations are most optimal to maximise the energy output.

1.4 Research questions

- Compared to monofacial PV, how have the bifacial PV market segmentation and price developed in the last five years?
- How does a dynamic albedo value affect the irradiation on a bifacial PV module compared to a static albedo value?
- How does the availability of albedo data affect the developed model performance?
- What tilt and azimuth angle maximise the energy output for the bifacial PV systems in Västerås?
- What economic savings and earnings does the optimal configuration yield?

1.5 Scope and delimitations

The developed model was limited to a single stand-alone PV module and does not include row to row shading. Due to the lack of available data from installed PV systems, the validation was limited to the Bifacial Experimental Single-Axis Tracker (BEST) -field located at the National Renewable Energy Laboratory (NREL) Campus in Denver, Colorado, USA. The validation of model performance was based on the front and rear irradiance due to insufficient information about the installed PV modules. The data available refer to seven monitoring months, from October 2019 to April 2020.

2 METHOD

In this chapter, the model development methodology is presented. Summarised method steps are shown in the schematic flow chart in Figure 2. Since this study had a deductive approach, the first step was to develop a theoretical framework from the literature study. The framework includes researching mathematical modelling and market development for bifacial PV. The second step was to develop the OptiCE code to include bifacial PV modules and validate the developed model. The third step was to evaluate how the albedo value affects the model performance based on three different albedo values. A case study of a bifacial PV single-axis tracker system located in Denver, USA, was used in this step. The fourth step was to analyse the optimal configurations to maximise the energy output of two installed bifacial PV system for the second case study of the farm Kärrobo Prästgård in Västerås, Sweden.

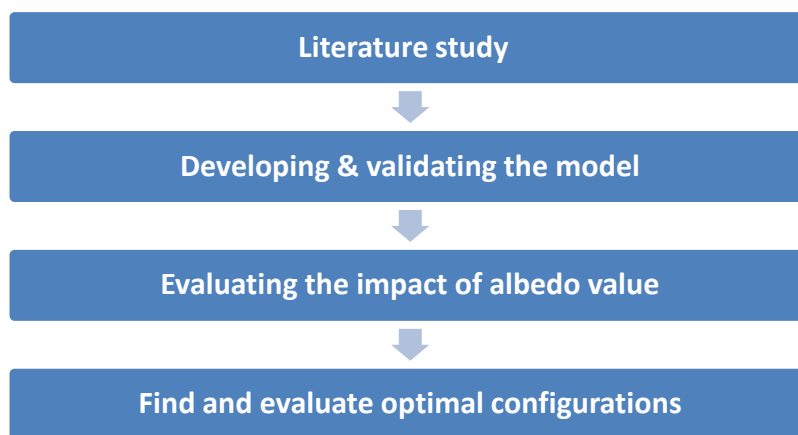


Figure 2 Schematic flow chart of the methodology.

2.1 Literature study

The literature research was based on gaining more knowledge about bifacial PV systems and the essential parameters from previously conducted research. Systematic literature research on state of the art was performed to describe the PV market development of bifacial modules. The monofacial price development was used as a comparison. The research focused on retrieving peer-reviewed information from google scholar, ScienceDirect and Primo (Mälardalen University library's search service). Keywords such as *albedo*, *bifacial photovoltaic module*, *modelling photovoltaics*, *PV module price*, *PV cell technology* and *Matlab* were used throughout this study.

2.2 Developing and validating the model

The developed bifacial PV model was implemented in the open-source code OptiCE, written in Matlab language (OptiCE, n.d.). Matlab is a software and programming language that enables mathematical and technical computations (Mathworks, n.d.a). The developed model

uses weather data and installation information to simulate the front and rear irradiance for a bifacial PV module. OptiCE functions and PV module parameters were used in the developed model to calculate the energy output. The developed model is further described in section 4.1 *Model framework*. The developed model was based on equations retrieved from PVLIB ToolBox and various scientific articles. PVLIB Toolbox is a set of open-source modelling functions available for Matlab and Python (Stein, Holmgren, Forbess, & Hansen, 2016). The Matlab version of PVLIB is available on the PV Performance Modelling Collaborative website (PVPMC Sandia, n.d.).

One site with installed bifacial PV modules was used to validate the model: the NREL Bifacial Experimental Single-Axis Tracker (BEST) field in Denver, USA. The validation was done by comparing the experimental irradiation data, measured at the site, with the model's simulated irradiation result. The data available refer to seven monitoring months, from October 2019 to April 2020. A single-axis tracker system was included in the developed model to simulate the BEST field site. The single-axis tracker equations were retrieved from the PVLIB toolbox (PVPMC Sandia, n.d.). For the simulations at NREL BEST-field in Denver, the weather and experimental data were available at the data hub DuraMAT (Ayala & Deline, 2020a; Ayala & Deline, 2020b). The weather and experimental data included measured front and rear irradiation, sun radiation, albedo values and installation configurations, as axis rotation and azimuth angles. The validation of the model was limited to measured data of the single-axis tracker system since the two systems at Kärro Prästgård (another site in Västerås, Sweden) was recently installed, and measured data was not available.

To further validate the model's performance, the result was compared with simulations in PVsyst. The software tool PVsyst enables the evaluation of different PV systems (PVsyst, n.d.c). PVsyst has developed a bifacial model for a single-axis tracker that is based on a 2D view-factor model. Asgharzadeh et al. (2019) evaluated the accuracy of PVsyst and three other bifacial irradiance models. The result indicated that the evaluated 2D bifacial models estimate the bifacial gain with about 1% absolute accuracy. PVsyst were chosen for this study due to availability.

Performance metrics as R^2 , RMSE, MAE and MBE were used when evaluating the model performance. Table 2 shows the formulas for the coefficient of determination (R^2), root mean square error (RMSE), mean absolute error (MAE) and mean bias error (MBE). The R^2 value range from 0 to 1 (or 0% to 100%), with a higher value indicating better goodness of fit² for the observations (Glen, n.d.; Grace-Martin, n.d.). The RMSE indicates how close the observed data is to the predicted values and a lower value means a better fit (Grace-Martin, n.d.). The MAE is used to measure forecast accuracy, and a smaller value is usually better. However, the RMSE and MAE performance is dependent on the average value of the data. If the RMSE or MAE is much lower than the average value of the data, then the accuracy is considered better. If the RMSE or MAE is similar to the average value, the accuracy is considered inferior (Vandepuut, 2019). MBE describes the direction of the error of the

² Comparison of observed data with the expected data (Kéry & Royle, 2016).

predicted values. If it is negative, then the predicted data is, on average, underestimated compared to the measured data and vice versa (AgriMetSoft, 2019).

Table 2 Performance metrics (Vännman & Jonsson, 2020; Willmott, 1982).

Name	Formula*
Coefficient of Determination	$R^2 = 1 - \frac{\sum_{i=1}^n (\hat{y}_i - \bar{y}_i)^2}{\sum_{i=1}^n (y_i - \bar{y}_i)^2}$
Root Mean Square Error	$RMSE = \sqrt{\frac{1}{n} \sum_{i=1}^n (\hat{y}_i - y_i)^2}$
Mean Absolute Error	$MAE = \frac{1}{n} \sum_{i=1}^n \hat{y}_i - y_i $
Mean Bias Error	$MBE = \frac{1}{n} \sum_{i=1}^n (\hat{y}_i - y_i)$

*Where \hat{y} is the predicted value of y , \bar{y} is the mean of y and n is the number of observations.

2.3 Evaluation of the impact of albedo value

When evaluating how the dynamic and static albedo value affects the irradiation of a bifacial PV module, the dynamic albedo value was divided into two different frequencies based on availability. The first albedo alternative were data for every hour measured at the site. The second was satellite-derived albedo, measured for every tenth day, to examine the accuracy of a model simulation without accessibility to advanced equipment. The static albedo, hereafter named as the fixed albedo value, was calculated at the site. The NREL BEST-field case study was used in the evaluation due to the available measured albedo values. Measured albedo data at Kärro Prästgård was not available for a sufficient period.

The hourly albedo values and fixed value were downloaded from the data hub DuraMAT (Ayala & Deline, 2020a; Ayala & Deline, 2020b). Satellite-derived albedo values for Denver was retrieved from the Copernicus global land service. Copernicus is a European programme that focuses on delivering open satellite earth observations (Copernicus, n.d.a). One of their programs is the Copernicus global land service, which delivers qualified bio-geophysical products on the land surface's status and evolution. The service can monitor the surface reflection of the earth for specific locations, and the spatial resolution is 1x1 km (Copernicus, n.d.b; Lellouch et al., 2020).

2.4 Find and evaluate optimal configurations for Kärro Prästgård

An optimisation tool was incorporated into the developed mathematical model to evaluate what system configurations maximise the energy output for the installed PV systems at Kärro Prästgård. The OptiCE open-source code has an existing optimisation function based

on genetic algorithms (GA) and will be used to retrieve optimal configurations (OptiCE, n.d.). The genetic algorithm is a function of the Optimisation Toolbox in Matlab (MathWorks, n.d.b). The optimisation of energy output was done by changing two parameters, the tilt and azimuth angle, which were chosen due to inspiration from previous research. The optimisation result was then compared with the output of the installed configurations that the developed model generated. The evaluation of the results was made by comparing the economic savings from selling electricity surplus and using self-produced electricity. The comparison was conducted with both a fixed albedo and an hourly albedo.

Hourly albedo was not possible to retrieve from the site at Kärro Prästgård due to availability. The hourly albedo data was calculated for a grass area in Roskilde, Denmark. The ground-reflected irradiance and global horizontal irradiance for the grass area was downloaded from the data hub DuraMAT (Marion, 2020a). Albedo calculations from a grass area in a similar climate as Kärro Prästgård was considered acceptable for this study.

The installed configurations, as tilt angle, azimuth angle, and module elevation, were retrieved by visiting the site of Kärro Prästgård. For the simulations at Kärro Prästgård, the weather data, which includes sun radiation, ambient temperature, and wind speed, was retrieved from SMHI and STRÅNG, which are open data sources (SMHI, n.d.a; SMHI, n.d.b). The site at Kärro Prästgård has installed two bifacial PV systems with two different module types. The module types are Jolywood 380W bifacial frameless module (JW-D72N-380M) and LONGi Solar 370W bifacial PERC module (LR4-60HBD-370M). Solar cell parameters for the installed modules were retrieved from datasheets by the manufacturers (LONGi Solar, 2020; EnergyPal, n.d).

The electricity consumption and electricity cost of the farm were required to evaluate the optimisation results. The load profile was provided by the farmer at Kärro Prästgård, Ulf Andersson. The optimisation was made for the entire year of 2020 to include all seasons. The economic data used to assess economic savings were based on the electricity spot price, taxes and fees related to Kärro Prästgård. The spot price was retrieved at Nord Pool (2021). The fixed fees in electricity cost were not considered since they do not vary on the electricity consumption. Investment costs and operation costs were not included in the optimisation since it was assumed that changing the tilt and azimuth angles of the systems would be the same.

3 LITERATURE STUDY

Previous studies regarding PV technologies, performance metrics and modules' price development are summarised in this chapter. Further, the impact of albedo on bifacial PV systems, system configurations and other factors that affect the performance are presented. Finally, a review of previous works conducted with OptiCE and genetic algorithms are described.

3.1 PV technologies

3.1.1 Bifacial PV

The commercialisation and mass production of bifacial modules started in the 2010s using various crystalline silicon (c-Si) bifacial PV cell structures (Liang et al., 2019). c-Si dominate the PV cell market 2020 with about 95% market share (Fischer et al., 2021). Common types of c-Si cells are PERL (passivated emitter rear locally diffused), PERC (passivated emitter rear contact), PERT (passivated emitter rear totally diffused), IBC (interdigitated back contact) and SHJ (silicon hetero-junction). The PERL/PERT/PERC market share was about 80% in 2020 (Fischer et al., 2021). SHJ cells stood for 2 - 3% of the market share but are forecasted to increase to 18% by 2031. Bifacial PERC cell technology can also be named PERC+, a schematic illustration of the cells shown in Figure 3 (Dullweber et al., 2015). The bifacial cells can accept light from the rear side since the technology only require metallisation of a proportion on the backside (Stein et al., 2021).

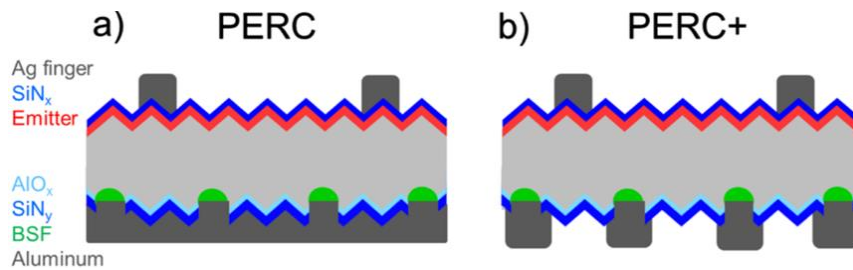


Figure 3 Schematic drawing of (a) an industry-typical monofacial PERC cell and (b) a bifacial PERC+ cell (Dullweber et al., 2015). Reprinted with permission.

Although bifacial PV modules stood for 17% of the market share during 2020, bifacial cells stood for 28% (Fischer et al., 2021). The gap in market share between bifacial cells and modules is because bifacial cells can be used in bifacial and conventional monofacial modules. Thus, 11 % of the bifacial cells are used in monofacial PV modules. For a bifacial cell in a monofacial glass-back-sheet PV module, illustrated in Figure 4(b), the white back sheet acts as a reflector for the cell (Dullweber et al., 2015). In bifacial PV modules, the cell's rear side is either encapsulated glass or a transparent polymer back sheet supported by an aluminium frame (Singh, Gou, Peters, Aberle, & Walsh, 2015; Stein et al., 2021). Bifacial glass-glass PV modules can also be frameless, meaning they are manufactured without an

aluminium frame. The bifacial glass-glass module in Figure 4(a) shows how the light can reach the cell through both the module's front and rear sides.

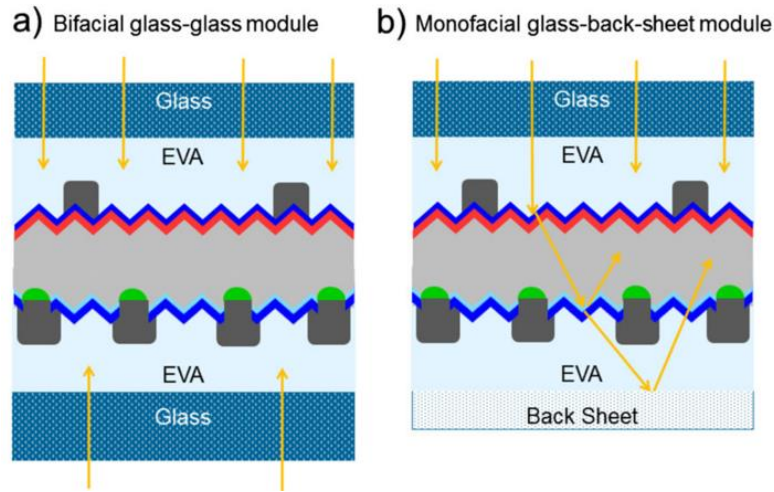


Figure 4 Schematic drawings of the bifacial PERC+ cell in (a) bifacial glass-glass PV modules and (b) monofacial PV modules with a white back sheet (Dullweber et al., 2015). Reprinted with permission.

3.1.2 Cell technologies

c-Si cell technology is also called the "first generation" of solar PV technologies (Sundaram, Benson, & Mallick, 2016, Chapter 2). Sundaram et al. (2016) describe the technology as mature with well-developed mass production. The cell technology also has a reasonable price and good efficiency (NREL, n.d.a). Table 3 summarises the front and rear efficiency and bifacial factor (BF) of different c-Si cell technologies. According to IEC 60904-1-2 standards, the bifaciality factor is $P_{mp,rear}/P_{mp,front}$ at standard test conditions (STC), where P_{mp} is the maximum power (Liang, Praveetoni, Singh, Wang, & Khoo, 2018). However, sometimes the bifacial factor (or bifaciality) is defined as the ratio of the rear side efficiency to the front side efficiency (Deline et al., 2017). The efficiencies depend on the surroundings of measurements, complicating a comparison between different bifacial cells.

Table 3 Efficiency and bifaciality factor of c-Si cell technologies.

	Front-side efficiency	Rear-side efficiency	Bifacial factor	Reference
PERC	21.2 - 22.7%	15.4 - 18.6%	69 - 82%	(Dullweber et al., 2015; Zhang et al., 2020; Hu et al., 2019; Bellini, 2017)
PERL	19.8%	17.6%	89%	(Lohmüller et al., 2017)
PERT	18.6 - 23.2%	15.3 - 18.6%	80 - 87.5%	(Teppe et al., 2015; Bellini, 2019; Wei et al., 2017; Mihailetschi et al., 2015)
IBC	20.9 - 22%	15.6 - 18.3%	74 - 83%	(Guillevin et al., 2017; Mihailetschi et al., 2015)
SHJ	17.9%	16.0%	89.6%	(Chowdhury et al., 2021)

In addition to c-Si cells, there are other types of developed solar cells with varying efficiencies. These can be divided into second and third-generation (Sundaram et al., 2016). The second generation is thin-film technology. The cells are made from very thin semiconductor materials to reduce the material and energy consumption (NREL, n.d.a; Sundaram et al., 2016). Sundaram et al. (2016) summarise the main technologies in thin-film technologies: copper indium gallium selenide, cadmium telluride and amorphous silicon. Multijunction solar cells based on III-V materials have high efficiency but are not considered cost-effective due to high production costs and the low abundance of cell technology components. Lee and Ebong (2017) state that thin-film solar cells show promise in competing with c-Si technology within efficiency due to minimal material usage. In contrast, Fisher et al. (2021) assume that the market share of thin-film cells will remain at 5%. Little progress in implementing bifacial technology in thin-film cells has been made, according to Phillips et al. (2020), due to high back surface recombination velocity. The surface recombination velocity is seemed to be an important parameter since it affects the dark saturation current and quantum efficiency of solar cells (Markvart & Castañer, 2017).

The third-generation solar cells aim to use environmentally friendly materials and reduce manufacturing costs (Sundaram et al., 2016). The leading technologies in the third generation are dye-sensitized, organic and perovskite solar cells. Perovskite/c-Si tandem solar cells have emerged in recent years by achieving an efficiency of 28 - 30% (NREL, n.d.b; Hutchins, 2020b). However, perovskite/c-Si tandem cells are still in research stages and have not yet been commercialised (Li & Zhang, 2020). Tandem configurations are designed to absorb the entire solar light range and include two or more cells (Wali, Elumalai, Iqbal, Uddin, & Jose, 2018). Lehr et al. (2020) found that bifacial perovskite/c-Si tandem PV modules can increase the energy yield by 18 - 23% compared to monofacial tandem perovskite/c-Si modules. And by 24 - 38% compared to bifacial c-Si PV modules.

3.1.3 PV system performance metrics

The specific yield is a commonly used performance metric for solar PV systems is according to Zhang (2017a). It is mainly used to analyse the difference between PV designs or compare suitable locations for PV systems. The specific yield is the energy produced in kWh divided by the kWp of module capacity and is often calculated over a year. Zhang also mentions factors that impact the specific yield. Zhang concludes that the chosen location is the main influencing factor. The exposure of shade, soiling and snow cover are factors related to the location. Further factors that influence the specific yield is the weather file used in simulations, module orientation and module selection. The balance of system efficiency concerning the inverter efficiency, current losses, mismatch losses, and inverter clipping affects the specific yield.

Leloux et al. (2015) found that the mean annual specific yield in the United Kingdom, Belgium, France, and Spain was 898, 908, 1115 and 1450 kWh/kWp. The systems investigated were of different sizes, PV technologies and orientations. The authors discussed that factors, such as newly emerged technologies, would be interesting to add in future research to update the results. Baumann et al. (2018) evaluated an east-west oriented vertical

bifacial PV system at a rooftop site in Switzerland. The result showed that the system had an annual specific yield of 942 kWh/kWp from August 2017 to August 2018. Schelin (2019) conducted a degree project to evaluate existing PV systems' specific yield in Sweden. Results showed that the annual specific yield of PV systems in Sweden ranged from 602-955 kWh/kWp during 2017 and 681-1015 kWh/kWp during 2018, with the southern systems ranging higher than the northern systems. The PV systems in region Västmanland had an annual mean specific yield of 745 kWh/kWp for 2017 and 867 kWh/kWp 2018.

Molin, Stridh, Molin and Wäckelgård (2018) found that a vertical east-west oriented bifacial PV system in Sweden had an annual specific yield of 990 kWh/kWp from 2016 to 2017. In addition, the authors evaluated a monofacial PV system with a south-facing orientation close to the bifacial system. They found that it had an annual specific yield of 980 kWh/kWp during the same period. The authors also evaluated two systems at another experimental site with south-oriented bifacial and monofacial PV systems, both with a 40° tilt. They found that the annual specific yield for the south-oriented bifacial PV system was 1000 kWh/kWp, and for the monofacial PV system, the annual specific yield was 950 kWh/kWp.

3.2 Market price development

The price of PV modules has decreased over time. According to IRENA (2020), a decrease of 87% to 92% has been seen from 2009 to 2019, depending on the c-Si module type. The decline mainly depended on five factors; continued improvement in module efficiency, reduced material uses in manufacturing processes, decreased labour cost with more efficient manufacturing methods, economies of scale and increased competition between suppliers. Lusson (2020) discuss bifacial modules and that the technology may claim a significant market share of the solar PV market in the future. However, one crucial factor is the cost. In Figure 5, data from PVinfoLink (n.d.) and bifacial manufacturers shows that the price for bifacial modules and monofacial high-performance modules have closed in on each other in the global market. In addition to the increased production of bifacial modules, the decreased cost gap leads to more available data and improved design, according to Lusson. However, factors such as different designs, site location and challenging installations compared to monofacial systems may create problems for investors and affect widespread adoption.

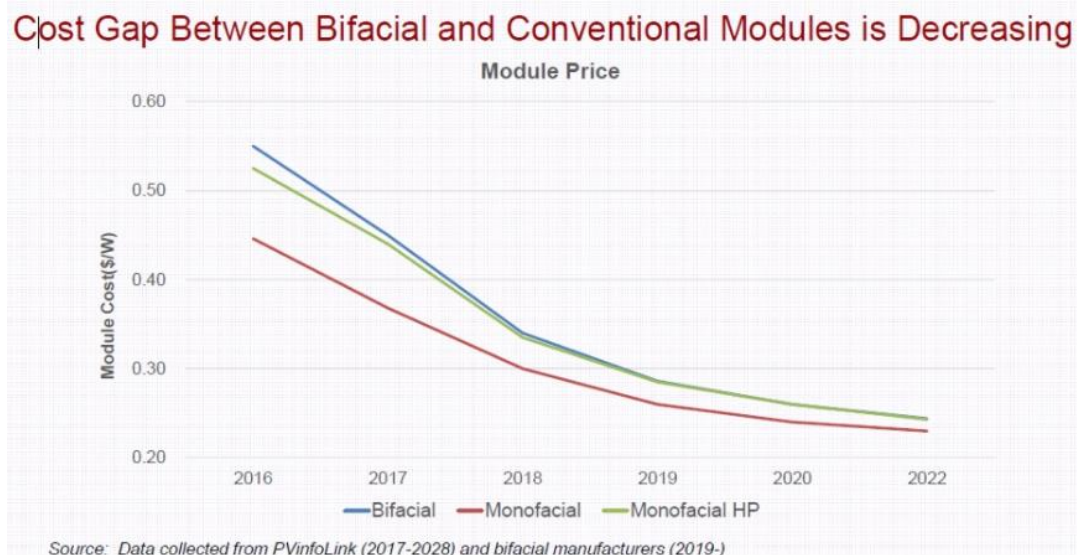


Figure 5 Cost gap between bifacial and conventional modules (Lusson, 2020; PVInfoLink, n.d.). Reprinted with permission.

The global deployment of bifacial modules emerged in 2019. In December 2019, the average price for a bifacial module was 0.38 €/W_p in Europe (IRENA, 2020; Schachinger, 2021). In Figure 6, Schachinger (2021) summarised how the price for bifacial modules closed in on high efficiency and all-black modules during 2020 on the EU spot market.

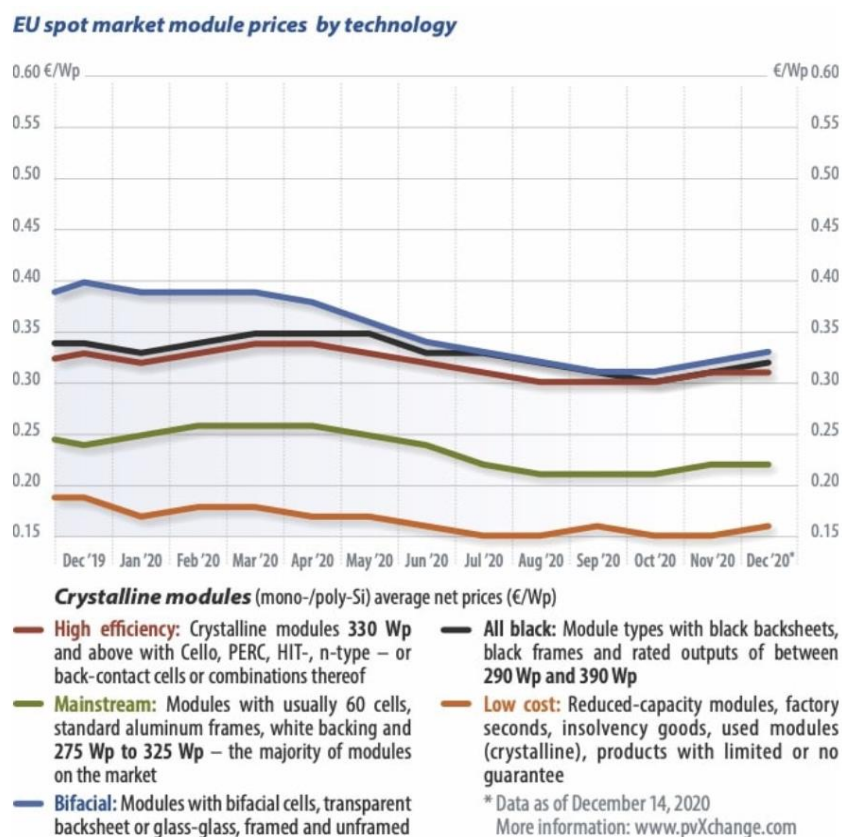


Figure 6 EU spot market module prices by technology (Schachinger, 2021; pvXchange, 2020). Reprinted with permission.

Woodhouse et al. (2019) compared the manufacturing cost between monofacial PERC modules with bifacial PERC, n-PERC/PERL and SHJ based on glass-glass technology, illustrated in Figure 7. It showed that in 2019, a 375W monofacial PERC module and a 365W bifacial PERC module had a 6% difference in module cost. The monofacial PERC module had an average manufacturing cost of \$0.31/W_{DC}, and the bifacial PERC module \$0.33/W_{DC}. The cost components with the highest impact on the manufacturing cost were the bill of materials, remaining direct manufacturer costs for cell conversion, and wafers' price. The n-PERC/PERL module cost \$0.35/W_{DC} and had a similar cost component dependence as the PERC modules. The SHJ module showed the highest manufacturing cost, varying between \$0.35 - 0.38/W_{DC}, with a higher remaining direct manufacturer cost for cell conversion than the other technologies. The wafer price and bill of materials costs were similar for all of the different cell technologies.

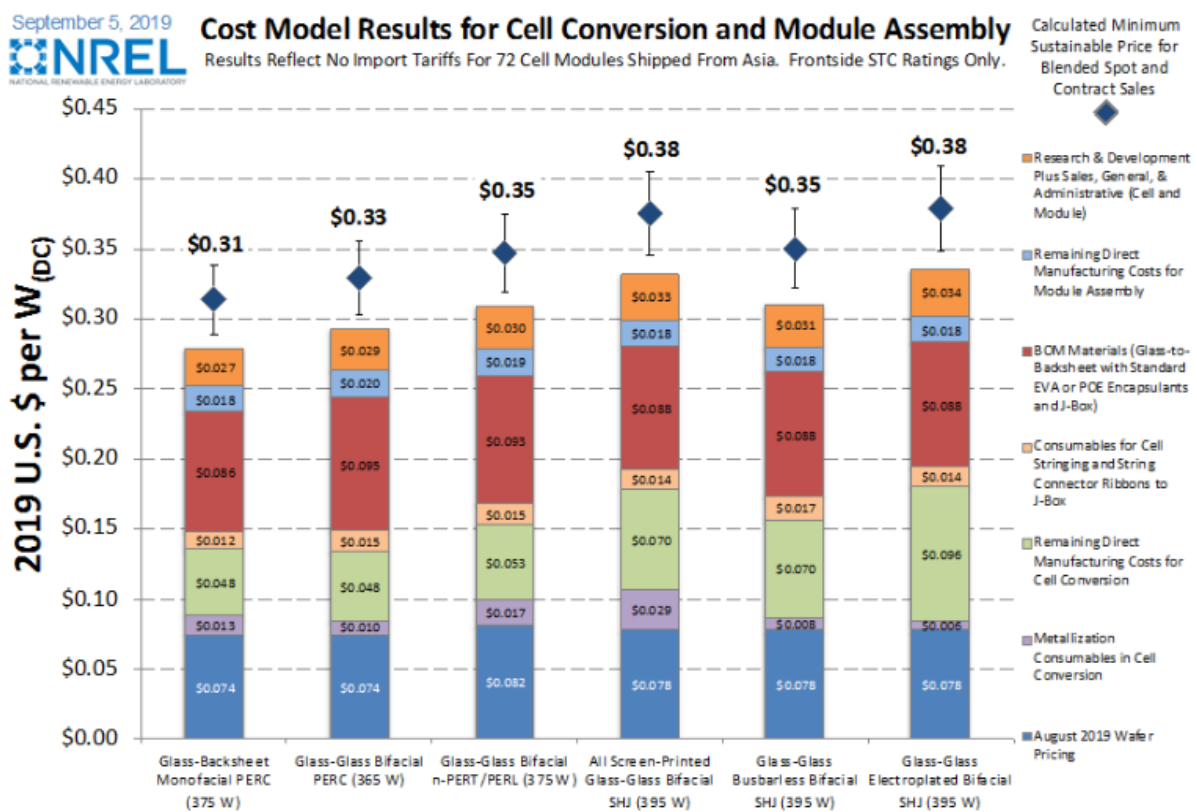


Figure 7 Cost model results for cell conversion and module assembly (Woodhouse et al., 2019). Reprinted with permission.

3.3 The albedo value

3.3.1 The impact on ground-reflected irradiance

The surface albedo has long been under assessment by various researchers. Dickinson (1983) describes that the albedo is generally dependent on both the wavelength and incident angle of

incoming solar radiation. Surface albedos are dependent on the surface textures and structures as well as composition. Molin et al. (2018) state that the albedo value significantly influences the bifacial PV energy yield. They conclude that a higher ground albedo will increase the energy yield. Sun et al. (2018) found that the bifacial gain increased by 20% when comparing a ground-mounted bifacial PV module with albedo 0.25 to a module elevation height of 1 m and albedo 0.5.

The albedo effect on the energy yield was analysed by Chiodetti et al. (2016). The authors compared the energy yield simulated by a bifacial PV system that used both a variable albedo and a fixed albedo. The results showed that a fixed albedo overestimated the total energy yield compared to a variable albedo. Since the variable albedo considered factors such as solar zenith angle, the diffuse ratio, and the influence of rain, it was more accurate. Chiodetti et al. also investigated how fixed albedo values of 0.2, 0.4, and 0.6 affected the ground-reflected (albedo) irradiance of a bifacial module's front and rear side. The result showed that the diffuse and beam irradiation on the front and rear side were not affected by an increased albedo while the ground-reflected irradiance increased. For the rear side, the ground-reflected irradiance increased significantly, while for the front side, the increase was minor. Zhang, Wang, Pan and Hu (2012) examined diurnal albedo variations and concluded, as Chiodetti et al., that surface albedo is higher in the morning than in the afternoon when the solar elevation angle is less than 40°. The up-facing parabolic curve of diurnal surface albedo was caused by solar elevation angle under clear sky conditions.

3.3.2 Albedo measurements

Reliable albedo data is essential to estimating a bifacial PV systems's energy yield (Chiodetti et al., 2016). Hutchins (2020a) explained that onsite measured albedo is essential for accurate simulations when evaluating bifacial projects. Calculating the albedo can be done with two horizontal pyranometers, one facing the ground and the other facing the sky (Marion, 2020b). The albedo is the irradiance measured by the ground-facing pyranometer divided by the irradiance measured by the sky-facing pyranometer (Lave, 2015), shown in equation (1).

$$\rho = \frac{\text{Ground reflected irradiance}}{\text{Global horizontal irradiance}} = \frac{I_{GRI}}{I_{GHI}} \quad (1)$$

3.3.3 Albedo modelling

Measured albedo at the location is considered more reliable but requires advanced equipment (Marion, 2021). Marion (2021) found that satellite-derived albedos can be used cautiously to evaluate bifacial PV systems' performance. It is possible to retrieve satellite-derived albedo measurements at the Copernicus Global Land Service (Copernicus, n.d.b). The available data in the Copernicus Global Land Service is divided into bi-hemispherical and directional-hemispherical reflectance, which is also called white-sky albedo (ρ^{ws}) and black-sky albedo (ρ^{bs}), respectively. Wang et al. (2015b) describe the difference between white-sky and black-sky albedo. White-sky albedo is dependent on the isotropic incident

irradiation, which is independent of direction and assumes 100% diffuse irradiation. The black-sky albedo is dependent on direct irradiation and solar geometry (Ω_i). Solar geometry involves solar zenith and azimuth angles.

The albedo of a surface that considers the white- and black-sky albedo is known as the blue-sky albedo (Lewis & Barnsley, 1994; Wang et al., 2015b). The blue-sky albedo (ρ) is presented in equation (2) and depends on the fraction of diffuse irradiation. The diffuse fraction (f_{diff}) is the ratio of the diffuse horizontal irradiation (I_{DHI}) to the global horizontal irradiation (I_{GHI}).

$$\rho(\Omega_i) = \rho^{ws} \cdot f_{diff} + \rho^{bs}(\Omega_i) \cdot (1 - f_{diff}) \quad (2)$$

Diurnal variation of albedo can be estimated using the solar zenith angle as the dominant variable (Dickinson, 1983). Briegleb, Minnis, Ramanathan and Harrison (1986) presented an approach to estimate the direct-beam surface (black-sky) albedo based on the work of Dickinson (1983), shown in equation (3).

$$\rho^{bs}(\theta_z) = \rho_0 \cdot \frac{1 + C}{1 + 2 \cdot C \cdot \cos(\theta_z)} \quad (3)$$

where θ_z is the solar zenith angle, ρ_0 is the albedo under direct illumination at $\theta_z = 60^\circ$, C is a constant depending on the surface type (0.4 for arable land, grassland and desert, and 0.1 for all other types) (Briegleb et al., 1986). Wang, Zeng, and Barlage (2007) proposed that the C value could be obtained by minimizing the difference between measured and computed albedo values. The authors recommend a new set of C values in their report (0.26 for grasslands). Yang et al. (2008) stated that the albedo under direct illumination at solar zenith angle 60° varies depending on the surface type, geographical location and season. Grant, Prata and Cechet (2000) evaluated the estimation of the daily mean albedo with equation (3) using different ways to estimate C and ρ_0 ; fixed or fitted for each day. The authors found that determining the C and ρ_0 values for each day gave a higher simulation accuracy of the albedo compared to fixed values. Wang et al. (2007) stated that the white-sky albedo is independent of the solar zenith angle and thus can be obtained by integrating equation (3) over all solar zenith angles, shown in equation (4).

$$\rho^{ws} = \rho_0 \cdot \frac{1 + C}{C} \left(1 - \frac{1}{2 \cdot C} \ln(1 + 2 \cdot C) \right) \quad (4)$$

Chiodetti et al. (2016) evaluated the Briegleb et al. (1986) approach and presented a mathematical method to estimate the albedo, shown in equation (5). The mathematical model is an adaption of equation (2).

$$\rho(\theta_z) = \rho^{ws} \cdot f_{diff} + \rho_0 \cdot \frac{1 + C}{1 + 2 \cdot C \cdot \cos(\theta_z)} \cdot (1 - f_{diff}) \quad (5)$$

Chiodetti et al. (2016) stated that the unknown parameters of equation (5) (which are C , ρ_0 and ρ^{ws}) can be found by fitting the model to onsite measurements. According to the authors, only a few days or weeks of measurements are theoretically necessary for the model to adapt

to various irradiation conditions. The global RMSE of the mathematical method was reported to be 6.6% for concrete and 5.5 % for grassland.

3.4 System configurations & surrounding factors

Asgharzadeh et al. (2018) stated that the optimal tilt of a south-facing bifacial PV module is complicated to estimate since it depends on the albedo, module elevation, size, weather conditions and season. Various researchers have studied vertical tilted modules with a tilt angle of 90° . Guo, Walsh and Peters (2013) compared the minimum albedo required to get a higher performance of a vertical bifacial PV module than a monofacial PV module for different latitudes. The result showed that for lower latitudes, the minimum required albedo is higher than for higher latitudes. Wang et al. (2015a) concur with Guo et al. (2013). that the latitude of where the bifacial module is installed influences energy yield. As the sun elevation angle decreases with higher latitude, they conclude that a bifacial PV module has higher performance at locations with low sun elevation angles. The authors argue that the required module elevation depends on the latitude. The result showed that a lower module elevation is sufficient at higher latitudes compared to lower latitudes. Results were due to the self-shadowing effect directly underneath the module.

Sun et al. (2018) estimated that a south-north-facing optimal tilted bifacial PV module has higher bifacial gain across the globe than an east-west vertical bifacial PV when ground-mounted with an albedo of 0.25. The optimally tilted bifacial PV modules were optimised for maximum production. However, when increasing the albedo to 0.5, the authors found that the ground-mounted east-west vertical bifacial PV can have higher bifacial gain than the south-north-facing optimal tilted bifacial PV module below the latitude of 30° . For latitudes above 30° , the result was reversed. Sun et al. also compared the two module setups for module elevation of 1 meter and albedo 0.5. They found that when elevating the two meters to 1 meter, the south-north suffers less from self-shading and can produce more power than the east-west. Thus, the south-north facing becomes again optimal. Appelbaum (2016) supports these results by studying the identical two setups at a latitude of 32° . The south-north-facing module produced 32 % more energy than the east-west facing module.

Appelbaum (2016) found that vertical collectors are more sensitive to row-to-row shading than tilted collectors due to the height. However, the author adds that more vertical collectors than tilted collectors can be installed in the same area. Nonetheless, if the row pitch is too small, it will increase the row-to-row shading. Self-shading is a part of the shadowing effect and can lead to significant losses for a PV module (Masters, 2004). Asgharzadeh et al. (2018) state that the increased shadowing effect on large-scale bifacial PV, compared to single module systems, generates a lower energy output in the centre module. The shadowing effect includes horizon blocking, diffuse sunlight blocking from surrounding modules, and area shadowing cast by modules on the ground. The shadowing effect can include the row pitch and row distance, where the row pitch is the distance between the module centre of two PV rows. The distance between the back edge of the first row and the second row's front edge is the row distance. The row pitch is equal to the row distance for vertically installed modules.

Shoukry et al. (2016) conducted a study regarding the row distance effect on the energy yield for a setup of three rows. Results showed that a small distance between the rows decreased the bifacial gain in the centre modules compared to the outer layer.

Hajjar, Dubaikel and Ballard (2015) showed that vertical collectors are less affected by soiling, which affect energy production and cost, in climates with high dust accumulation. Granlund, Narvesjö and Petersson (2019) show in their study, conducted in Sweden at latitude 65°N, that snow soiling has less impact on vertical modules than lower tilts. With snow-covered ground, it is possible to achieve high albedo values. Chen, Li, Li and Liu (2014) found that the snow albedo is relatively high (0.7-0.9) for fresh snow. However, the snow albedo decreases exponentially with time after the snowfall.

3.5 OptiCE and genetic algorithms in previous research

The open-source code OptiCE is used to design, simulate, and optimise off-grid applications (OptiCE, n.d.). The OptiCE model focuses on integrating clean energy technologies in microgrids or as distributed generation in larger grids. It has been continuously developed to include solar photovoltaic (PV), wind turbine, diesel generator and battery bank for off-grid applications, and power-to-heat conversion technologies and storage systems. The open-source code is based on Matlab language and uses a GA for optimisation problems. Campana, Zhang, Lundblad, Li and Jinyue (2017) evaluated the capabilities of the open-source code. They described it as a tool, which can be used for more than ten clean energy technologies with several operational strategies. Additionally, since OptiCE is based on Matlab, the end-user can customise the simulation, optimisation and operational strategies. Campana et al. pointed out that further development of the open-source code involves integrating further models and validating the models and optimisation techniques.

GA is an optimisation and search method which adapts and evolves depending on genetic processes similar to biological organisms (Beasley, Bull, & Martin, 1993). According to Beasley et al. (1993), a close reference would be the principles of natural selection and "survival of the fittest". The GA can, with suitable encoding, adopt this principle and "evolve" solutions to real-world problems. However, this artificial evolution method is much more simplified than real natural evolution, but GAs' have shown a capability to solve surprisingly complex design problems (Renner & Ekárt, 2003). Similar to the real world, Beasley et al. explain that GAs' consist of a population of "individuals" that each represent a possible solution for a given problem. Each individual is assigned a fitness score according to how well it fits the solution objective. The individuals with higher scores are then "mated" to form the next generation of individuals. Meanwhile, the individuals with lower scores will most likely not be used for reproduction, so they will "die out". This process will continue to converge and find the optimal solution to the problem. Renner et al. conclude that genetic algorithms are flexible and adapted to different design and optimisation problems. For example, Merei, Berger and Saur (2013) used a genetic algorithm to investigate the optimised configuration of a hybrid system. The system consisted of PV panels, a wind turbine, batteries for energy storage and a backup diesel generator.

Several studies on PV systems have used OptiCE and GA to find optimal solutions for various objectives. Campana et al. (2015) performed an economic optimisation of a photovoltaic water pumping system for irrigation, which was conducted based on three decisional variables. The variables included PV power peak capacity, tilt angle, and surface azimuth angle. By combining the dynamics of the PV water pumping system, crop water demand, and groundwater level and using the optimisation function in OptiCE, the system's efficiency increased. Additionally, the investment cost was reduced. The results showed a 10% increase in PV power output during the irrigation period with the optimised tilt and azimuth angles compared to the existing orientation. The PV size was also reduced from 1.44kW_P to 0.96kW_P. Campana et al. (2016) developed an MS Excel-VB program based on the OptiCE model to optimise the capacity of solar home systems components. The focus was to minimise costs and maximise the self-sufficiency of the system. The results showed that the developed model was a powerful tool for designing optimal configurations of solar home systems based on a given load profile. The original Matlab based model was in good agreement with the optimisation results of the developed Excel program.

Zhang et al. (2017b) used OptiCE to compare a single diode PV model, a simplified model, and two different battery models. The objective was to maximise the self-sufficiency ratio and maximise the net present value based on three decisional variables. The three variables included component capacity, PV azimuth angle and PV tilt angle. Results showed that a single-diode model was more favourable than the simplified model since the simplified model tended to overestimate production compared to the single-diode model. Another report studied the optimisation of floating PV systems for shrimp farm cultivation in Thailand (Campana, Wästhage, Nookuea, Tan, & Yan, 2019). The study included a dynamic techno-economic approach and evaluated different types of PV and wind-based hybrid systems. It was based on simulations and optimisations to minimise the LCOE while maximizing the energy system self-sufficiency. Decisional variables such as tilt angle, azimuth angle, PV capacity, wind tower height, wind power capacity and battery capacity were used. Results showed that a hybrid energy system with PVs' represented the best solution for the selected location. The hybrid energy system with PVs' was favourable due to the abundance of solar irradiation compared to available wind resources.

4 MODEL AND CASE STUDIES

In this chapter, the model framework and the theories used when developing the mathematical model are explained. Further, two different cases are presented. In the first case, the NREL BEST-field was used to validate the developed model and study the effect of dynamic and static albedo. In the second case, Kärrobo Prästgård was used to evaluate the optimal system configurations for maximum energy output.

4.1 Model framework

The model is based on OptiCE (n.d.), and the overall model framework of the developed model is presented in Figure 8. The model's input is the system configuration, irradiance, albedo, weather data, and module characteristics. OptiCE is used to calculate the solar position and power. The developed model uses the inputs and solar position to calculate the incidence angle, reflection losses and irradiance components. The steps in the OptiCE and the developed model will be presented and explained throughout section 4.2 *Front and Rear Irradiance* and 4.3 *Power generation*.

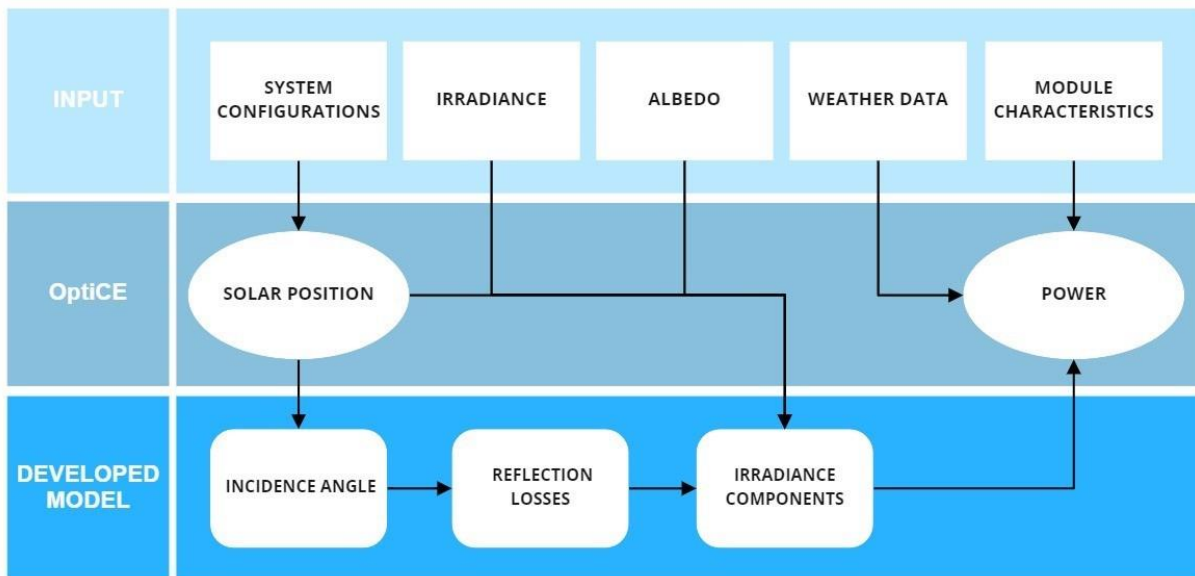


Figure 8 Overall model framework.

4.2 Front and Rear Irradiance

The total solar irradiance is the sum of the total beam irradiance (I_{beam}), diffuse irradiance (I_{diff}) and ground-reflected (albedo) irradiance (I_{alb}) on the surface, seen in equation (6) (Duffie & Beckman, 2006). The beam, ground-reflected and diffuse components can be seen in Figure 9. The diffuse irradiance consists of diffuse isotropic, diffuse circumsolar and diffuse horizon brightening.

$$I_{tot} = I_{beam} + I_{diff} + I_{alb} \quad (6)$$

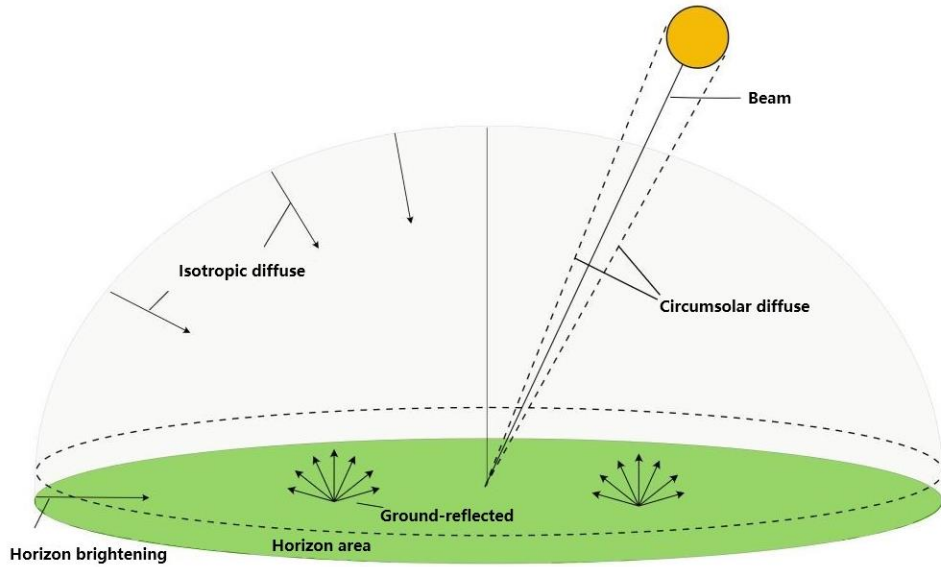


Figure 9 Solar irradiance components (own illustration, inspiration from Duffie & Beckman (2006)).

4.2.1 Solar and PV module angles and directions

The position of the sun and the orientation of the module can be expressed in angles (Duffie & Beckman, 2006). Figure 10 is a schematic illustration that shows some of the angles. The solar position can be described with the solar azimuth angle (γ_s) and solar altitude angle (α_s). The irradiation onto the PV module will depend on solar position, module azimuth angle (γ) and module tilt (β). The solar zenith angle (θ_z) is defined as $90 - \alpha_s$.

For a bifacial PV module, the five components are computed for both the front and rear surface to find the front and rear irradiance. When calculating the rear irradiance, the module tilt and module azimuth angles are corrected with 180 degrees: $\gamma_R = \gamma_F + 180$ and $\beta_R = 180 - \beta_F$. Where F and R stand for "Front" and "Rear", respectively. The tilt (β) in Figure 10 refers to the front tilt (β_F).

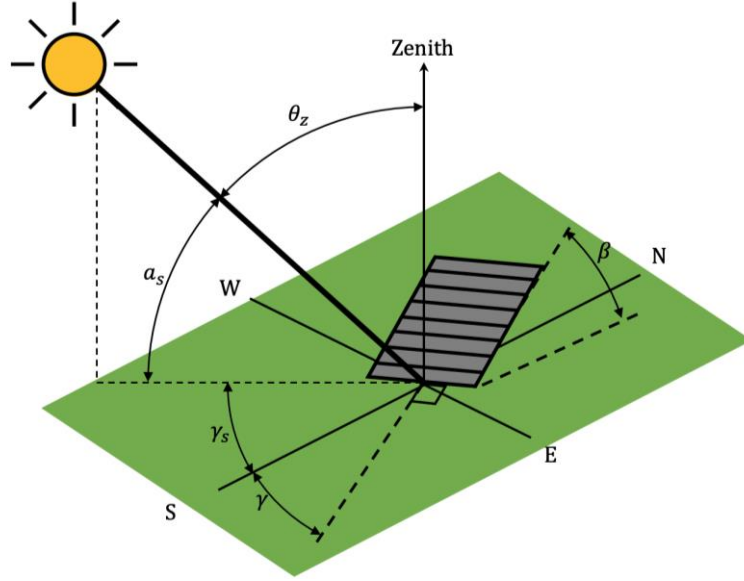


Figure 10 Angles of PV module (own illustration, inspiration from Duffie & Beckman (2006)).

The angle of incidence (θ) is the angle between the beam radiation on a surface and the normal to that surface. Equation (7) expresses the angle of incidence related to the solar position and surface angles (Duffie & Beckman, 2006). The angle of incidence may exceed 90° , which means that the sun is behind the surface. It is therefore essential to assume that $\max(\theta_{F/R}) = 90^\circ$.

$$\cos \theta_{F/R} = \cos \theta_z \cdot \cos \beta_{F/R} + \sin \beta_{F/R} \cdot \sin \theta_z \cdot \cos(\gamma_s - \gamma_{F/R}) \quad (7)$$

To calculate the reflection losses of diffuse horizon irradiance, the horizontal angle of incidence (θ_{hor}) was computed. The computation is done with a solar zenith angle of 90° , and the azimuth angle is assumed to be linear at the horizon, and the horizon brightening is independent of the azimuth angle (thus $\gamma_s = \gamma$) (EnergyPlus, n.d.; Hooper & Brunger, 1980). The horizontal angle of incidence is estimated as follows:

$$\cos \theta_{hor,F/R} = \cos 90 \cdot \cos \beta_{F/R} + \sin \beta_{F/R} \cdot \sin 90 \cdot \cos(\gamma_{F/R} - \gamma_{F/R}) \quad (8)$$

4.2.2 Reflection losses

When calculating the front and rear irradiance, it is essential to account for reflection losses in each irradiance component. Martín and Ruiz (2002; 2004) presents the following equations that can be used to calculate the reflection loss for beam, horizontal, albedo, and isotropic irradiance.

$$R_{loss,beam}^{F/R} = \frac{\exp(-\cos \theta_{F/R} / a_r) - \exp(-1/a_r)}{1 - \exp(-1/a_r)} \quad (9)$$

$$R_{loss,hor}^{F/R} = \frac{\exp(-\cos(\theta_{hor,F/R}) / a_r) - \exp(-1/a_r)}{1 - \exp(-1/a_r)} \quad (10)$$

$$R_{loss,alb}^{F/R} = \exp \left[-\frac{1}{a_r} \left(c_1 \cdot \left(\sin \beta + \frac{\left(\frac{\pi \cdot \beta}{180} \right) - \sin \beta}{1 - \cos \beta} \right) + c_2 \left(\sin \beta_{F/R} + \frac{\left(\frac{\pi \cdot \beta}{180} \right) - \sin \beta}{1 - \cos \beta} \right)^2 \right) \right] \quad (11)$$

$$R_{loss,iso}^{F/R} = \exp \left[-\frac{1}{a_r} \left(c_1 \cdot \left\{ \sin \beta_{F/R} + \frac{\pi - \left(\frac{\pi \cdot \beta}{180} \right) - \sin \beta_{F/R}}{1 + \cos \beta_{F/R}} \right\} + c_2 \left\{ \sin \beta_{F/R} + \frac{\pi - \left(\frac{\pi \cdot \beta_{F/R}}{180} \right) - \sin \beta_{F/R}}{1 + \cos \beta_{F/R}} \right\}^2 \right) \right] \quad (12)$$

where a_r is the angular loss coefficient, and c_1 and c_2 are fitting parameters. Typical values applicable for a silicon PV module are $a_r = 0.16$, $c_1 = 4/3\pi$ and $c_2 = -0.074$ (Martín & Ruiz, 2002).

4.2.3 Direct beam irradiance

The direct beam irradiance is estimated with the direct normal irradiance (I_{DNI}) on both the front and rear side of the module, shown in equation (13).

$$I_{beam,F/R} = I_{DNI} \cdot \cos(\theta_{F/R}) \cdot (1 - R_{loss,beam}^{F/R}) \quad (13)$$

The global diffuse horizontal irradiance (I_{GHI}) can be expressed as the function of direct normal irradiance (I_{DNI}), diffuse horizontal irradiance (I_{DHI}) and solar zenith angle (θ_z); $I_{GHI} = I_{DNI} \cdot \cos(\theta_z) + I_{DHI}$.

4.2.4 Diffuse irradiance

The diffuse on the tilted surface is computed with the Perez model. Perez, Stewart, Seals and Guertin (1988) divides the diffuse irradiance into three parts, as shown in equation (14).

$$I_{diff} = I_{diff,iso} + I_{diff,cir} + I_{diff,hor} \quad (14)$$

Duffie and Beckham (2006) described the three diffuse irradiances. The isotropic irradiance ($I_{diff,iso}$) is received uniformly from the entire skydome. Circumsolar diffuse ($I_{diff,cir}$) is the result of the forward scattering of solar radiation and concentrated in the sky around the sun. While the horizon brightening ($I_{diff,hor}$) is concentrated near the horizon. The following equations give the diffuse irradiance on a tilted surface:

$$I_{diff,iso,F/R} = I_{DHI} \cdot (1 - F_1) \cdot \left(\frac{1 + \cos \beta_{F/R}}{2} \right) \cdot (1 - R_{loss,iso}^{F/R}) \quad (15)$$

$$I_{diff,cir,F/R} = I_{DHI} \cdot F_1 \cdot \frac{a_{F/R}}{b} \cdot (1 - R_{loss,beam}^{F/R}) \quad (16)$$

$$I_{diff,hor,F/R} = I_{DHI} \cdot F_2 \cdot \sin \beta_{F/R} \cdot (1 - R_{loss,hor}^{F/R}) \quad (17)$$

where F_1 and F_2 are the circumsolar and horizon brightness coefficients and $a_{F/R}$ and b are terms that account for the angle of incidence on the circumsolar radiation. (Perez et al., 1988) These variables are described with the limits:

$$a_{F/R} = \max(0^\circ, \cos \theta_{F/R}), b = \max(\cos 85^\circ, \cos \theta_z) \quad (18)$$

F_1 and F_2 can be estimated with equation (19) and (20) (Perez et al., 1988)

$$F_1 = \max \left[0, \left(f_{11} + f_{12} \cdot \Delta + \frac{\pi \cdot \theta_z}{180} \cdot f_{13} \right) \right] \quad (19)$$

$$F_2 = \left(f_{21} + f_{22} \cdot \Delta + \frac{\pi \cdot \theta_z}{180} \cdot f_{23} \right) \quad (20)$$

The coefficients are the function of three parameters that describe the sky condition: zenith angle (θ_z), clearness parameter (ε), and brightness parameter (Δ) (Perez et al., 1988). The brightness coefficients ($f_{11}, f_{12} \dots f_{23}$) can be collected from Table 4 with the clearness parameter.

$$\varepsilon = \frac{\left(\frac{I_{DHI} + I_{DNI}}{I_{DHI}} \right) + 1.041 \cdot \left(\frac{\pi \cdot \theta_z}{180} \right)^3}{1 + 1.041 \cdot \left(\frac{\pi \cdot \theta_z}{180} \right)^3} \quad (21)$$

$$\Delta = \frac{I_{DHI} \cdot m}{I_{Extra}} \quad (22)$$

where m is the air mass that can be estimated with equation (23) (Kasten & Young, 1989) and I_{DHI} is the diffuse horizontal radiation. I_{Extra} is the extra-terrestrial radiation incident on the plane normal to the radiation, calculated with equation (24).

$$m = 1 / (\sin(90 - \theta_z) + 0.50572 \cdot (6.07995 + \theta_z)^{-1.6364}) \quad (23)$$

$$I_{Extra} = SC \cdot (1.00011 + 0.0034221 \cdot \cos B + 0.001280 \cdot \sin B + 0.000719 \cdot \cos 2B + 0.000077 \cdot \sin 2B) \quad (24)$$

where SC is the solar constant, determined as 1361.1 W/m^2 by Gueymard (2018), and $B = (2\pi \cdot d)/365.242$, where d is the day of the year.

Table 4 Brightness Coefficients (data retrieved from Perez, Ineichen, Seals, Michalsky, and Stewart (1990)).

Range of ε	f_{11}	f_{12}	f_{13}	f_{21}	f_{22}	f_{23}
1,000 – 1,065	-0,008	0,588	-0,062	-0,060	0,072	-0,022
1,065 – 1,230	0,130	0,683	-0,151	-0,019	0,066	-0,029
1,230 – 1,500	0,330	0,487	-0,221	0,055	-0,064	-0,026
1,500 – 1,950	0,568	0,187	-0,295	0,109	-0,152	-0,014
1,950 – 2,800	0,873	-0,392	-0,362	0,226	-0,462	0,001
2,800 – 4,500	1,132	-1,237	-0,412	0,288	-0,823	0,056
4,500 – 6,200	1,060	-1,600	-0,359	0,264	-1,127	0,131
6,200 – ∞	0,678	-0,327	-0,250	0,156	-1,377	0,251

4.2.5 Ground-reflected irradiance

Sun et al. (2018) present a model for estimating the ground-reflected irradiance, shown in equation (25). The ground-reflected irradiance (I_{alb}) consider two types of self-shading losses. The first one is the direct blocking of the direct beam and circumsolar light by the module onto the ground. The second is the sky masking of isotropic diffuse light by the module. The model employs the view-factor approach.

$$I_{alb,F/R} = \left(I_{alb,F/R}^{diff,iso} + I_{alb,F/R}^{dir} + I_{alb,F/R}^{diff,cir} \right) \cdot \left(1 - R_{loss,alb}^{F/R} \right) \quad (25)$$

4.2.5.1 Reflected Isotropic Diffuse Irradiance

Sun et al. (2018) describe that only a fraction of isotropic diffuse irradiance from the sky hits the ground and reflects on the module due to the ground being shaded by solar modules. Self-shading caused by sky masking affects the ground-reflected irradiance on the module. The diffuse isotropic irradiance strongly depends on the ground position (x) from which the view factor is calculated. Figure 11 shows an illustration of the self-shading of ground-reflected light from isotropic diffuse light.

$$I_{alb,F/R}^{diff,iso} = \rho \cdot I_{alb,iso,grd} \cdot \frac{1}{H} \cdot \int_{x_{min}}^{+\infty} VF_{x \rightarrow sky}(x) \cdot VF_{x \rightarrow F/R}(x) dx \quad (26)$$

Equation (26) assumes an infinitely large ground reflector where ρ is the ground albedo coefficient, and H is the module height. The diffuse isotropic irradiance that reached the ground ($I_{alb,iso,grd}$) can be estimated with the Perez model with equation (15) by assuming $\beta = 0^\circ$ and $\gamma = 0^\circ$. The view factor ($VF_{i \rightarrow j}$) is the fraction of the radiation leaving surface i that strikes surface j directly (Cengel, 2002). The integration of ground-reflected irradiance collected by the module in equation (26) is over the view factor of x to the sky ($VF_{x \rightarrow sky}$) and the view factor of x to the front or rear side of the module ($VF_{x \rightarrow F/R}$). The integral is computed over the ground, defined with the limitations $x_{min} = \frac{E}{\tan(\beta_{F/R})}$ to infinity. $VF_{x \rightarrow sky}$ and $VF_{x \rightarrow F/R}$ is estimated with equation (27) and (28), respectively.

$$VF_{x \rightarrow sky} = 1 - \frac{\cos(\theta_{M1}) + \cos(\theta_{M2})}{2} \quad (27)$$

$$VF_{x \rightarrow F/R} = 1 - VF_{x \rightarrow sky} \quad (28)$$

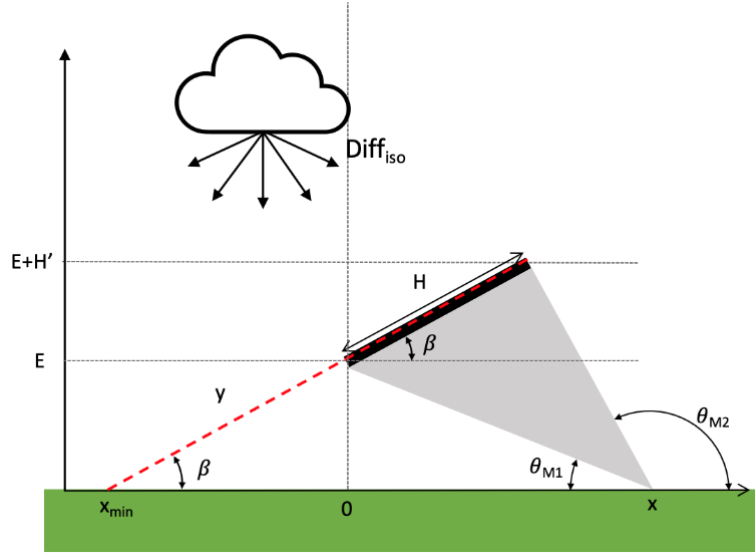


Figure 11 Self-shading of ground-reflected light from isotropic light ($Diff_{iso}$) (own illustration, inspiration from Sun et al. (2018)).

As shown in Figure 11, the masking angles, θ_{M1} and θ_{M2} , represent the angle between the normal of shadow (ground) and module, respectively. The two angles can be calculated with equation (29) and (30). E is the module elevation and H is the module height.

$$\theta_{M1} = \begin{cases} 180 + \cot^{-1}\left(\frac{x}{E}\right), & x < 0 \\ \cot^{-1}\left(\frac{x}{E}\right), & x \geq 0 \end{cases} \quad (29)$$

$$\theta_{M2} = \begin{cases} -\cot^{-1}\left(\frac{x - H \cdot \cos(180 - \beta_{F/R})}{E + H \cdot \sin(180 - \beta_{F/R})}\right), & x < H \cdot \cos(180 - \beta_{F/R}) \\ 180 - \cot^{-1}\left(\frac{x - H \cdot \cos(180 - \beta_{F/R})}{E + H \cdot \sin(180 - \beta_{F/R})}\right), & x \geq H \cdot \cos(180 - \beta_{F/R}) \end{cases} \quad (30)$$

4.2.5.2. Reflected Direct and Circumsolar Diffuse Irradiance

Parts of the direct and circumsolar diffuse irradiance on the ground do not reflect on the module due to self-shading, as shown in Figure 12.

$$I_{alb,F/R}^{dir} = \rho \cdot I_{DNI} \cdot \cos \theta_z \cdot VF_{F/R \rightarrow grd,ns}^{dir} \quad (31)$$

$$I_{alb,F/R}^{diff,cir} = \rho \cdot I_{alb,cir,grd} \cdot VF_{F/R \rightarrow grd,ns}^{cir} \quad (32)$$

where $V_{F/R \rightarrow grd,ns}^{dir}$ and $V_{F/R \rightarrow grd,ns}^{cir}$ is the direct and circumsolar view factor of the module's front or rear side to the not shaded ground, respectively. Estimating the fraction of the module to the ground (not shaded) can be done with the view factor. The diffuse circumsolar irradiance that reached the ground ($I_{alb,cir,grd}$) can be estimated with the Perez model, described in section 4.2.4 *Diffuse irradiance* with equation (16) by assuming $\beta = 0^\circ$ and $\gamma = 0^\circ$.

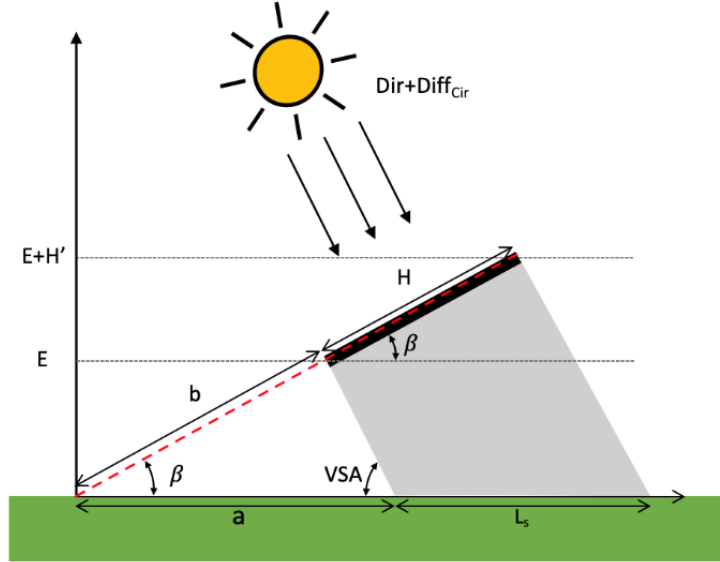


Figure 12 Self-shading of ground-reflected light from direct (*Dir*) and circumsolar diffuse light (*Diff_{cir}*) (own illustration, inspiration from Sun et al. (2018)).

The shadow length (L_s) depends on the solar position. The illustration in Figure 12 shows how the shadow length can be illustrated during a specific time. Where H is the module height, a is the distance between the shadow and origin³, and b is the distance between the module and origin.

$$L_s = H \cdot \sin(180 - \beta_{F/R}) \cdot \left(\frac{1}{\tan(VSA_{F/R})} + \frac{1}{\tan(\beta_{F/R})} \right) \quad (33)$$

where VSA is defined as the vertical shadow angle (or profile angle) (Duffie & Beckman, 2006).

$$VSA = \frac{\tan(90 - \theta_z)}{\cos(\gamma_s - (180 + \gamma_{F/R}))} \quad (34)$$

³ The point where the axis of a coordinate system intersect, where all coordinates are zero.

Appelbaum (2018) presents the view factor of the shaded ground to the rear side of the module. Figure 13 shows an illustration of the view factor computed in equation (35).

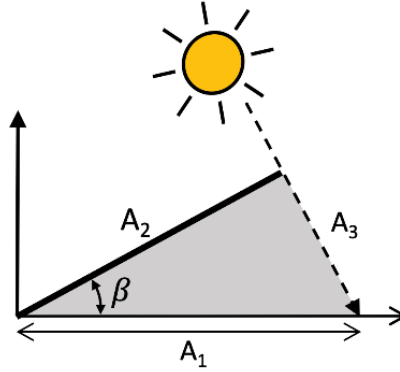


Figure 13 Illustration of view factor of the shaded ground (A_1) to the rear side of the module (A_2) (own illustration, inspiration from Sun et al. (2018)).

$$VF_{A_1 \rightarrow A_2, R} = \frac{A_1 + A_2 - A_3}{2 \cdot A_1} = \frac{A_1 + A_2 - \sqrt{(A_1 - A_2 \cdot \cos \beta)^2 + (A_2 \cdot \sin(\beta))^2}}{2 \cdot A_1} \quad (35)$$

Since equation (35) is the view factor of the shaded ground to the rear side of a ground-mounted module, it is necessary to compute the view factor in parts. The reciprocity rule and the superposition rule enable the calculation of the view factor of the shaded ground to the rear side of an elevated module (Cengel, 2002). A pair of view factor $F_{i \rightarrow j}$ and $F_{j \rightarrow i}$ are related to each other by the reciprocity rule: $A_i \cdot F_{i \rightarrow j} = A_j \cdot F_{j \rightarrow i}$. And according to the superposition rule: "the view factor from a surface i to surface j is equal to the sum of the view factor of surface i to the parts of surface j ", which means that $F_{i \rightarrow (j_1, j_2)} = F_{i \rightarrow j_1} + F_{i \rightarrow j_2}$. The view factor for an elevated module, as shown in Figure 12, is computed with equation (35) according to the code shown in Figure 14 with the following constraints:

$$VF_{L_s \rightarrow F/R}^{dir} = \begin{cases} f(L_s, H, a, b), & \theta_{F/R} > 0 \\ 0, & \theta_{F/R} \leq 0 \end{cases} \quad (36)$$

where L_s is the shadow length, H is the module height, a is the distance between the shadow and origin, and b is the distance between the module and origin.

```

%first part
VF1_1 = ViewFactor_Cross(a,H+b,Panel_Tilt);% a to H+b
VF2_1 = ViewFactor_Cross(a,b,Panel_Tilt); % a to b
VF3_1 = (VF1_1-VF2_1).*a ./H; % H to a

%second part
VF1_2 = ViewFactor_Cross(LS+b,H+b,Panel_Tilt); %LS+a to H+b
VF2_2 = ViewFactor_Cross(LS+a,b,Panel_Tilt); %LS+a to b
VF3_2 = (VF1_2-VF2_2).(LS+a)./H; % H to LS+a

%third part
VF= (VF3_2 - VF3_1).*H ./LS; % LS to H
VF(isnan(VF)) = 0;

function [VF] = ViewFactor_Cross(A1,A2,Panel_Tilt)
VF=(A2+A1-sqrt((A1-A2.*cosd(Panel_Tilt)).^2+(A2.*sind(Panel_Tilt)).^2))./(2.*A1);
VF(isnan(VF)) = 0;
end

```

Figure 14 Matlab code for calculating the view factor.

The view factor of the front or rear side of the module to the not shaded ground can be calculated with equation (37).

$$VF_{F/R \rightarrow grd,ns}^{dir} = VF_{F/R \rightarrow grd}^{dir} - VF_{L_s \rightarrow F/R}^{dir} \cdot \frac{L_s}{H} \quad (37)$$

where $VF_{F/R \rightarrow grd}^{dir}$ is the view factor of the module to the ground (shaded and not shaded) is estimated by $(1 - \cos \beta_{F/R})/2$ (Appelbaum, 2018). The view factor of the module to the not shaded ground of circumsolar irradiance ($VF_{F/R \rightarrow grd,ns}^{cir}$) is computed in the same way with equation (33) to equation (37) with one modification. The vertical shadow angle for circumsolar irradiance (VSA^{cir}) is calculated with the zenith angle of circumsolar diffuse light ($\theta_{z,cir}$) that is equal to θ_z with the maximum value of 85° .

$$\theta_{z,cir} = \begin{cases} \theta_z, & \theta_z < 85^\circ \\ 85^\circ, & \theta_z \geq 85^\circ \end{cases} \quad (38)$$

4.3 Power generation

Duffie and Beckman (2006) describe the I-V characteristics that were used when estimating the power output (P) from the front and rear irradiance, which is calculated from equation (40).

$$I_C = I_L - I_0 \left[\exp\left(\frac{V + I_C \cdot R_s}{a}\right) - 1 \right] - \frac{V + I_C \cdot R_s}{R_{sh}} \quad (39)$$

$$P = I_C \cdot V \quad (40)$$

where V is the voltage, I_C is the current and is calculated with equation (39), I_L is the light current, I_0 is the diode reverse saturation current, R_s is the series resistance, R_{sh} is the shunt

resistance and a is the modified ideality factor described as $a = (n \cdot k \cdot T_c \cdot N_s)/q$. Where n is the ideality factor, k is the Boltzmann's constant ($1.381 \cdot 10^{-23} \text{ J/K}$), T_c is the cell temperature, N_s is the number of cells in series, and q is the electronic charge ($1.602 \cdot 10^{-19} \text{ coulomb}$). The cell temperature is estimated with reference module temperatures measured during nominal operating cell temperature (NOCT) with the following equation (41) (Duffie & Beckman, 2006).

$$\frac{T_c - T_a}{T_{NOCT} - 20} = \frac{I_{tot}}{800} \cdot \frac{9.5}{(5.7 + 3.8 \cdot v)} \cdot \left[1 - \frac{\eta_c}{0.9}\right] \quad (41)$$

where T_a is the ambient temperature, T_{NOCT} is the module temperature at NOCT conditions, η_c is the efficiency of the module when converting incident radiation into electrical energy, v is the wind speed and I_{tot} is the incident solar radiation. Applying the one-diode method for bifacial PV modules, the front and rear irradiance are added to calculate the solar radiation (PVsyst, n.d.a; Liang et al., 2018). The rear radiance is weighted by the bifaciality factor (BF) and added to the front radiance as shown in equation (42).

$$I_{tot} = I_{front} + BF \cdot I_{rear} \quad (42)$$

4.4 NREL BEST field

The NREL Bifacial Experimental Single-Axis Tracker (BEST) -field site is located at the NREL South Table Mountain Campus (latitude = 39.7398° , longitude = -105.1728°) (Ayala & Deline, 2020b). Table 5 summarises the system characteristics of the installed system at BEST-field. The installed system has trackers with a backtracking algorithm and a ground coverage ratio of 0.35. The configurations in Table 5 were used when performing the simulations in PVsyst, and the albedo value was set to the fixed value.



Figure 15 Picture of the bifacial PV modules installed at NREL BEST-field (Ayala & Deline, 2020b). Reprinted with permission.

Table 5 PV system characteristics of BEST field (Ayala & Deline, 2020b).

Information	Value	Unit
System type	Single-axis trackers	
Site albedo	0.26	
Module mounting height	1.5	m
Array azimuth angle	180	°
Tracker angle limit	60	°
Capacity	75	kW

4.4.1 Hourly, satellite-derived and fixed albedo

The different albedo alternatives are plotted in Figure 16. The satellite-derived albedo is only available for specific periods: 23rd of October to 24th of November and 9th of March to 17th of April. The “white-” and “black-sky” satellite-derived albedo values were retrieved from Copernicus (n.d.b), and the “blue-sky” albedo was calculated with equation (2). The fixed albedo is the site albedo from Table 5. In Figure 16 and Figure 17, the different albedo alternatives are plotted. The first figure is over seven months, and the second figure is for five days in November 2019 to illustrate the hourly albedo variation.

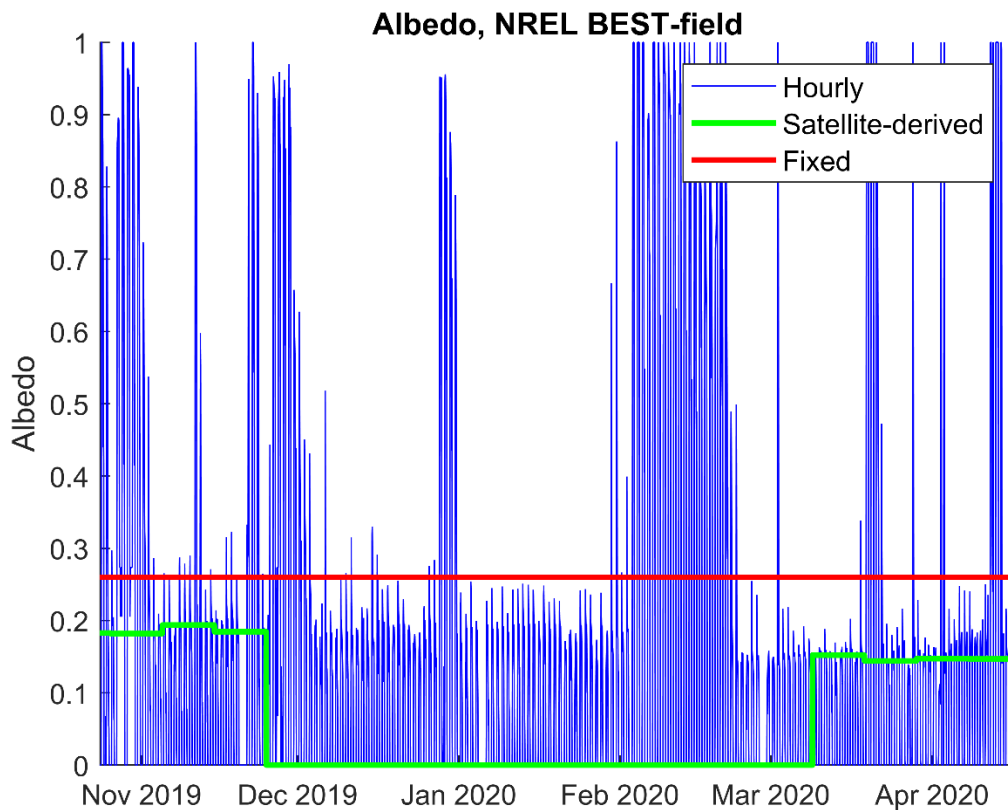


Figure 16 Albedo alternatives for seven months in 2019-2020 at NREL BEST-field.

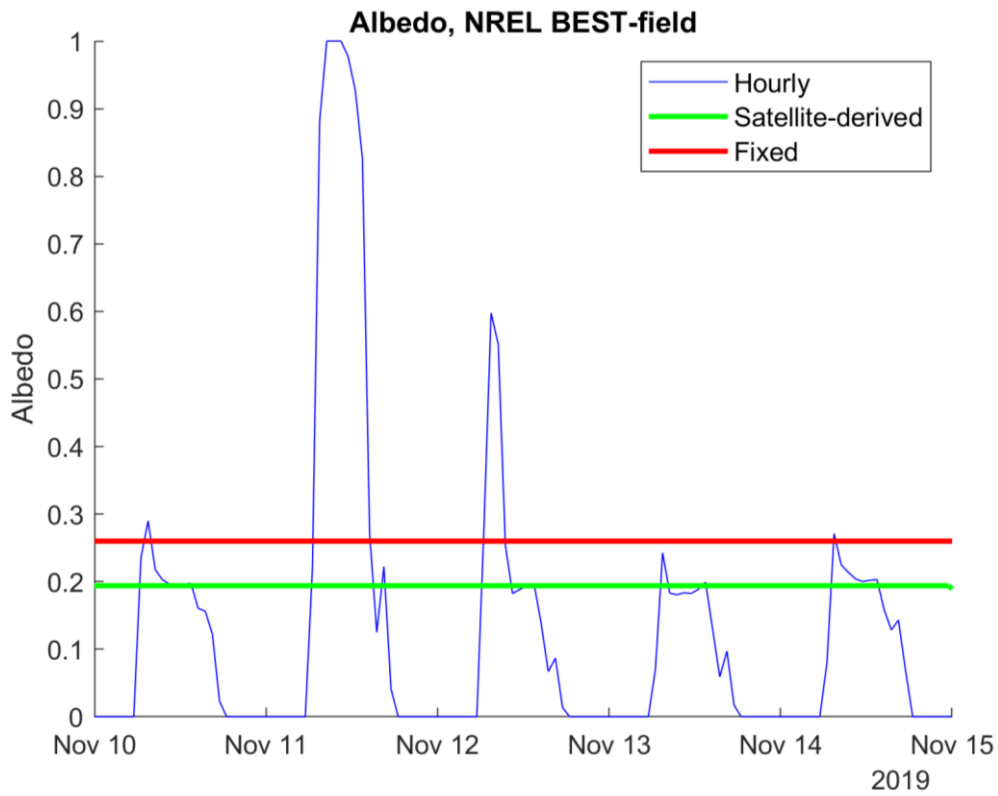


Figure 17 Albedo alternatives from the 10th to the 15th of November 2019 at NREL BEST-field.

4.5 Kärro Prästgård

The system at Kärro Prästgård is installed in Västerås, Sweden (latitude = 59.5549°, longitude = 16.7573°). At the farm, two bifacial PV systems have been installed on a grass field. Table 6 summarises the system characteristics of the installed systems at Kärro Prästgård. The site albedo will be assumed to 0.2 based on Table 1. The first installed system is a vertical system, and the second system is tilted, shown in Figure 18.



Figure 18 Picture of the vertical system (left) & reference system (right) installed at Kärro Prästgård.

Table 6 Characteristics of the installed systems at Kärro Prästgård.

Information	Vertical system	Reference system	Unit
System type	Fixed tilt	Fixed tilt	
Site albedo	0.2	0.2	
Module elevation	0.70	0.45	m
Front azimuth angle	-90* (East-West)	0 (South-North)	°
Front tilt angle	90	30	°
Capacity	22.8	11.84	kW
Module manufacturer	Jolywood	LONGi Solar	
Module type	JW-D72N-380M	LR4-60HBD-370M	

*Negative (-) azimuth angle = face towards the east.

4.5.1 Hourly and fixed albedo

The hourly albedo and the fixed albedo used for the site at Kärro Prästgård are illustrated in Figure 19 and Figure 20. The first figure is over the entire year, and the second figure is for five days in June 2019 to represent the hourly albedo variation. Both figures show that the hourly albedo tends to spike during the early and late hours. The hourly albedo was calculated from measured irradiation at a grass surface located in Roskilde, Denmark (latitude = 55.6964°, longitude = 12.1052°) (Marion, 2020c). The albedo was calculated with equation (1) from the ground reflected and global horizontal irradiance measured at the site. The irradiations were measured with SMP10 pyranometers (Marion, 2020c). The mean albedo value of the grass surface was 0.22. Snowfall was observed on six days: November 29th, December 14th, January 4th and, February 11th, 22nd and 26th.

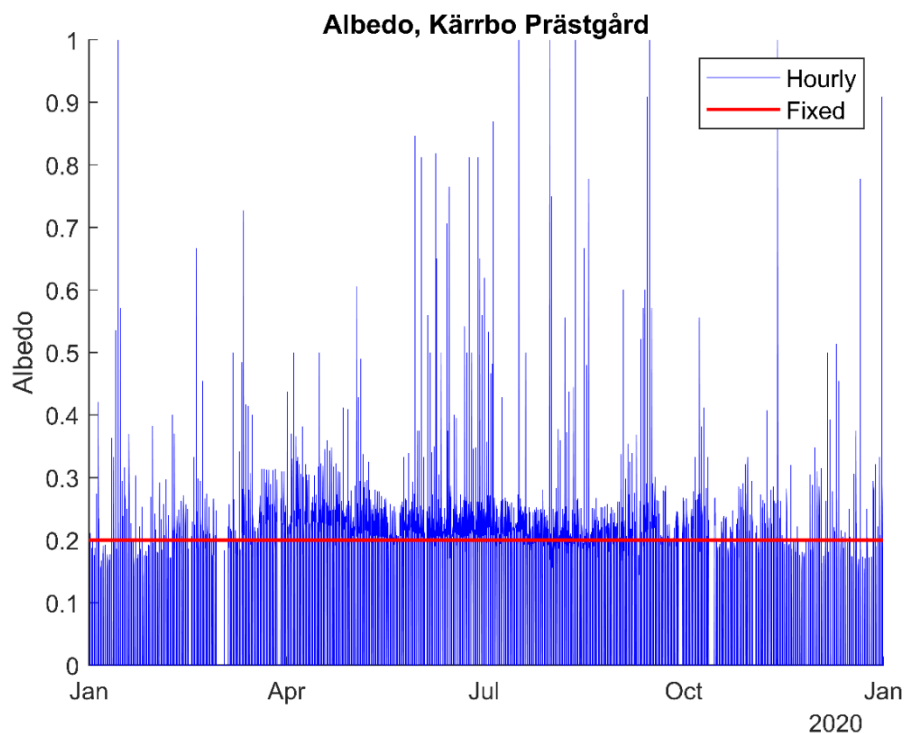


Figure 19 Hourly albedo from Roskilde and fixed albedo from Kärro Prästgård, for 2020.

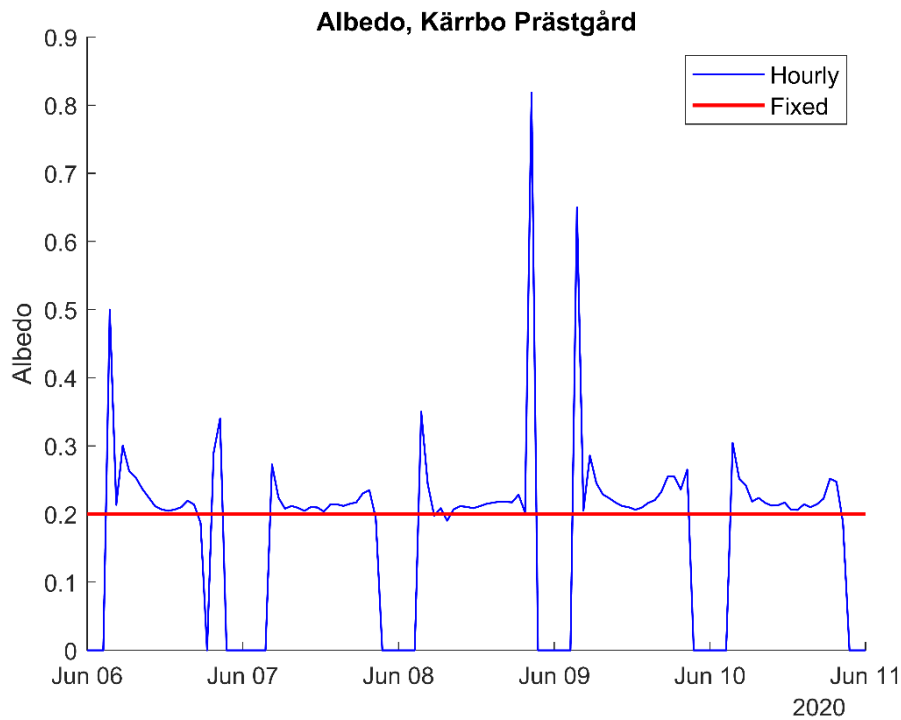


Figure 20 Hourly albedo from Roskilde and fixed albedo from Kärro Prästgård, for five days in June 2020.

4.5.2 Optimisation of system configurations

The optimisation aim was to maximise energy output based on changing the azimuth and tilt angle for the two bifacial PV systems installed at Kärro Prästgård. The specifics are given in Table 6. The boundaries of the system configurations for the optimisation are presented in Table 7.

Table 7 Boundaries of system configurations for optimisation.

	Vertically tilted	Reference system
Front tilt angle (°)	$\beta = 90$	$0 \leq \beta \leq 90$
Front azimuth angle (°)	$-180 \leq \gamma \leq 180$	$-180 \leq \gamma \leq 180$

The load curve of the farm Kärro Prästgård is shown in Figure 21, where the maximum consumption is set as 100%. The total electricity consumption for the farm was about 117 MW for 2020. With equation (44), this load can be calculated to cost about 60 906 SEK. As seen in Figure 21, there is insufficient data for the 13th of October. The electricity production of the PV system is balanced with the load of the farm. When electricity consumption is more significant than production by the PV system, there is an electricity shortage. The shortage is bought from the electricity trader. While at times that the production is more significant than the consumption, there is electricity surplus. The surplus is sold to the trader.

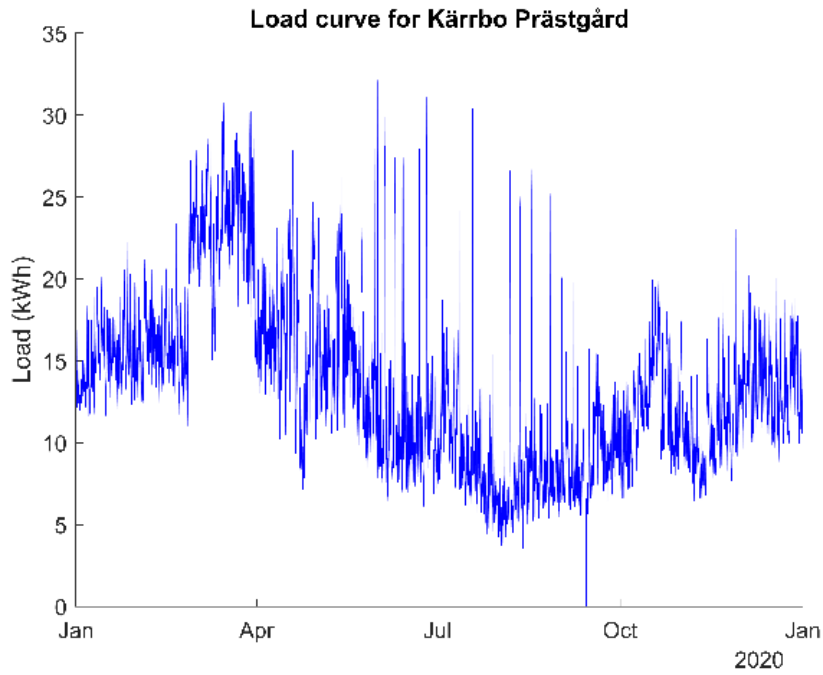


Figure 21 Graph of the electric hourly load curve for Kärrbo Prästgård, the year 2020.

4.5.3 Value of electricity

When calculating a solar system facility's payback time, the key components are the investment cost, operation and maintenance cost, and expected electricity costs and prices. The optimisation of tilt and azimuth angles at Kärrbo Prästgård are assumed to have similar investment costs and maintenance and operations costs. Thus, making the main difference between the revenue and savings for different installation configurations. The value of self-consumed solar electricity is equal to the price of bought electricity. Energimarknadsbyrån (2020a) summarized the essential components of self-consumed electricity and the value of sold and bought electricity, shown in equation (43), (44) and (45).

$$\text{Value of self-consumed electricity} = \text{Value of bought electricity} \quad (43)$$

$$\begin{aligned} \text{Value of bought electricity} = & \text{Monthly average spot price from Nord Pool} \\ & + \text{Surcharge from electricity trader} \\ & + \text{Transmission fee from DSO} \\ & + \text{Energy tax} \\ & + \text{Electricity certificate fee} \end{aligned} \quad (44)$$

$$\begin{aligned} \text{Value of sold electricity} = & \text{Monthly average spot price from Nord Pool} \\ & + \text{Repayment from DSO} \\ & + \text{Electricity certificate} \\ & + \text{Certificate of origin} \\ & + \text{Tax reduction} \end{aligned} \quad (45)$$

The price components are based on where the facility is located and the chosen electricity trader. Table 8 presents the input values used for the simulations at Kärrbo Prästgård. With

the assumptions that the company Vattenfall is the distribution system operator (DSO) and electricity trader. The energy tax for bought electricity is assumed to be 0.6 ÖRE/kWh since the farm pursues agriculture, enabling repayment of tax on electricity (Skatteverket, n.d.). The sold electricity includes a tax reduction is 60 ÖRE/kWh, a maximum of 30 000 kWh/year for main fuse rating contracts up to 100 A (Energimarknadsbyrån, 2020b). Figure 22 shows the monthly average spot price of electricity for 2020. However, the prices for 2020 was significantly lower than for 2018 and 2019 (Vattenfall, 2021c). Rydegran (2021) reported that the average system price for 2020 was 73% lower than for 2019 due to a mild winter season.

Table 8 Price of components.

Component	Price*
Surcharge	4 ÖRE/kWh excl. VAT
Energy tax	0.6 ÖRE/kWh excl. VAT
Transmission fee	48 ÖRE/kWh during high load time**, else 14.4 ÖRE/kWh
Repayment from DSO	8 ÖRE/kWh
Electricity certificate	0 ÖRE/kWh
Certificate of origin	1 ÖRE/kWh
Tax reduction	60 ÖRE/kWh (max 30 000 kWh/year)

* 100 ÖRE = 1 SEK = 0.11 USD (FOREX, 2021)

** High Load Time (HLT) is Monday to Friday 06-22 during November, December, January, February and March

Source: Data retrieved from Energimarknadsbyrån (2020a;2020b), Vattenfall (2021a; 2021b; 2021c; 2021d) and Skatteverket (n.d.).

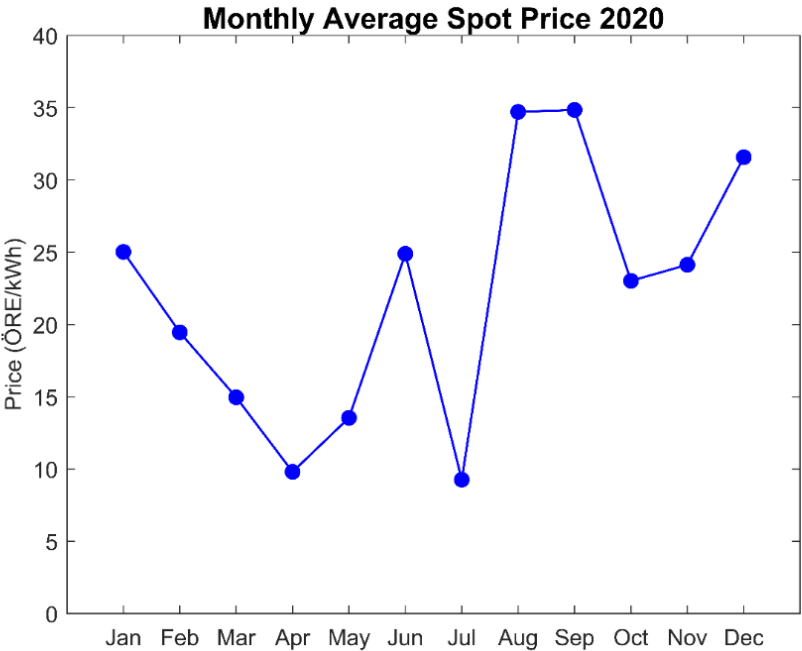


Figure 22 Monthly average spot price of electricity, the year 2020 (data retrieved from Nord Pool (2021)).

The value of bought and sold electricity for 2020 are calculated from equation (44) and (45), respectively, and shown in Figure 23. The sold electricity is higher since it includes the tax reduction while the bought electricity is calculated with repayments of energy tax. The

bought electricity is divided into high load time (HLT) and low load time (LLT), defined by the fee difference between hours of the day and season in Table 8.

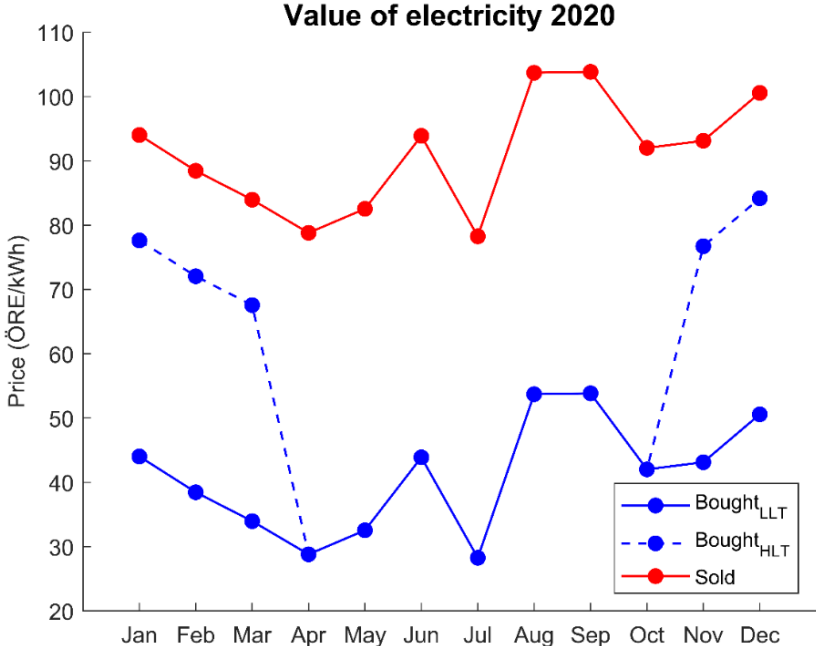


Figure 23 Calculated value of electricity for bought and sold electricity 2020 (HLT=high load time & LLT = low load time).

5 RESULTS

In this chapter, the results of the simulations conducted at NREL BEST-field and Kärrobo Prästgård are presented, including the validation, share of irradiance components, evaluation of albedo impact and optimisation.

5.1 Validation of the model: NREL BEST-field

Figure 24 shows scatterplots of the simulated irradiance at the NREL Bifacial Experimental Single-Axis Tracker field to the measured irradiance for the available data period: from the 23rd of October 2019 to the 17th of April 2020. The colour bar to the right represents the data's density, where yellow means that the number of data points in that area is high. (a-d) is the result of the simulations with the developed model, while (e-f) results from the simulations performed in PVsyst. The developed model with hourly albedo and fixed albedo gave a similar result to PVsyst for the front side of the module. While on the rear side, the developed model showed more accuracy than PVsyst. Additionally, the hourly albedo was more accurate than the fixed albedo for the rear side. The performance metrics for the simulations are summarised in Table 9.

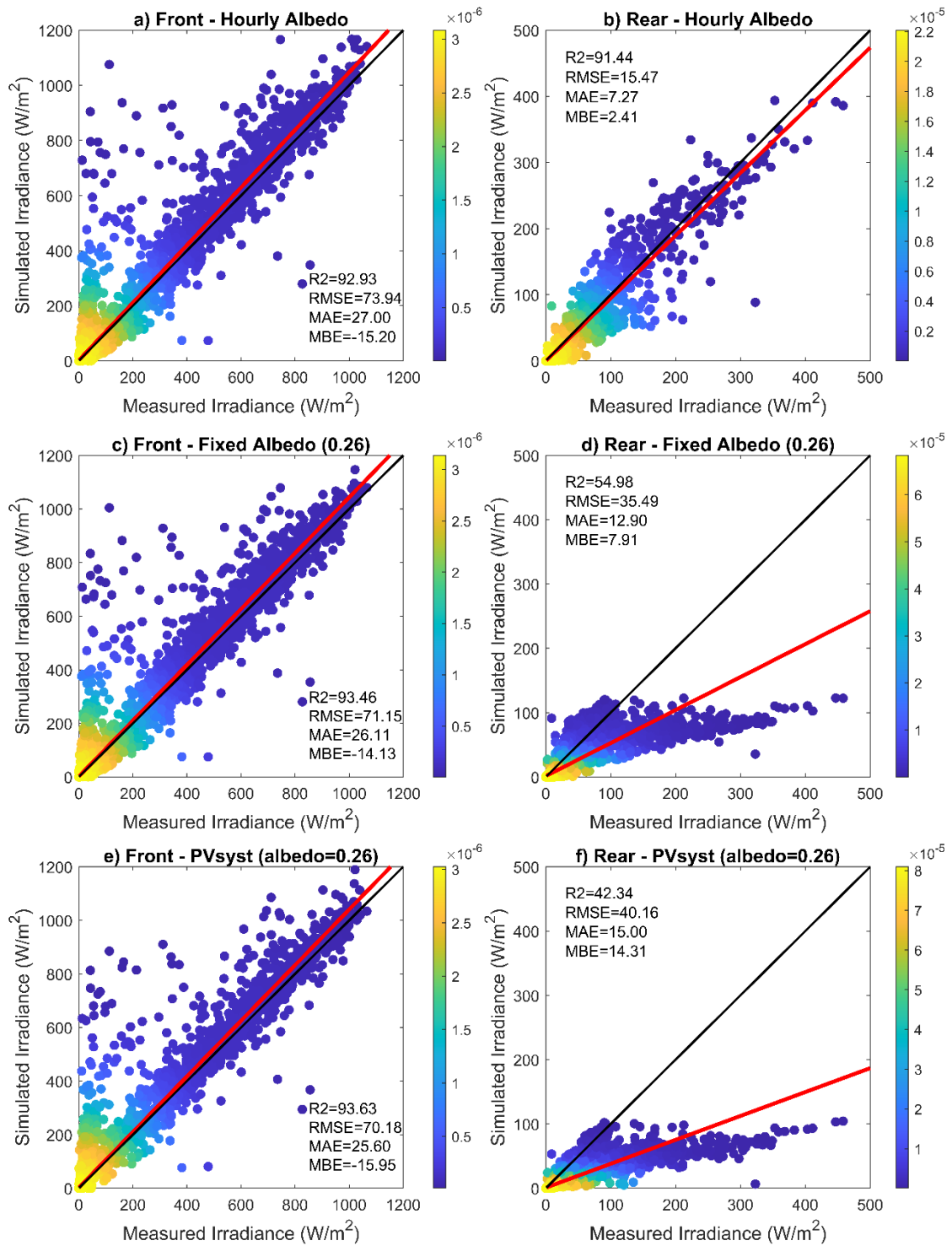


Figure 24 Scatterplots of front and rear irradiance with the developed model (hourly albedo in a-b and fixed albedo in c-d) and PVsyst (e-f, fixed albedo) - NREL BEST field, for Oct-Apr. The red line is a regression line, and the black line is an identity line ($f(x)=x$). (Note the different scale of the y-axis)

Table 9 Comparison of performance metrics from the developed model (hourly and fixed albedo) and PVsyst (fixed albedo) – NREL BEST field, for Oct-Apr.

	Front				Rear			
	R² (%)	RMSE (W/m ²)	MAE (W/m ²)	MBE (W/m ²)	R² (%)	RMSE (W/m ²)	MAE (W/m ²)	MBE (W/m ²)
<i>Hourly</i>	92.93	73.94	27.00	-15.20	91.44	15.47	7.27	2.41
<i>Fixed (0.26)</i>	93.46	71.15	26.11	-14.13	54.98	35.49	12.90	7.91
<i>PVsyst (0.26)</i>	93.63	70.18	25.60	-15.95	42.34	40.16	15.00	14.31

The total irradiance from the developed model (hourly and fixed albedo) and the simulated result with PVsyst are presented together with the measured irradiance in Figure 25. The total irradiance is divided into the front and rear sides' irradiance components for the simulations, while the measured irradiance is given in total. The front side has similar total irradiance of approximately 800 kWh/m² for simulations with the developed model as with PVsyst, as shown in Figure 24. In contrast, the hourly albedo gave total rear irradiation significantly larger than the simulations with fixed albedo and PVsyst. The figure clarifies that the rear ground-reflected irradiance is significantly impacted by the albedo value. In comparison, the total diffuse irradiance remains the same for both albedo alternatives with the developed model.

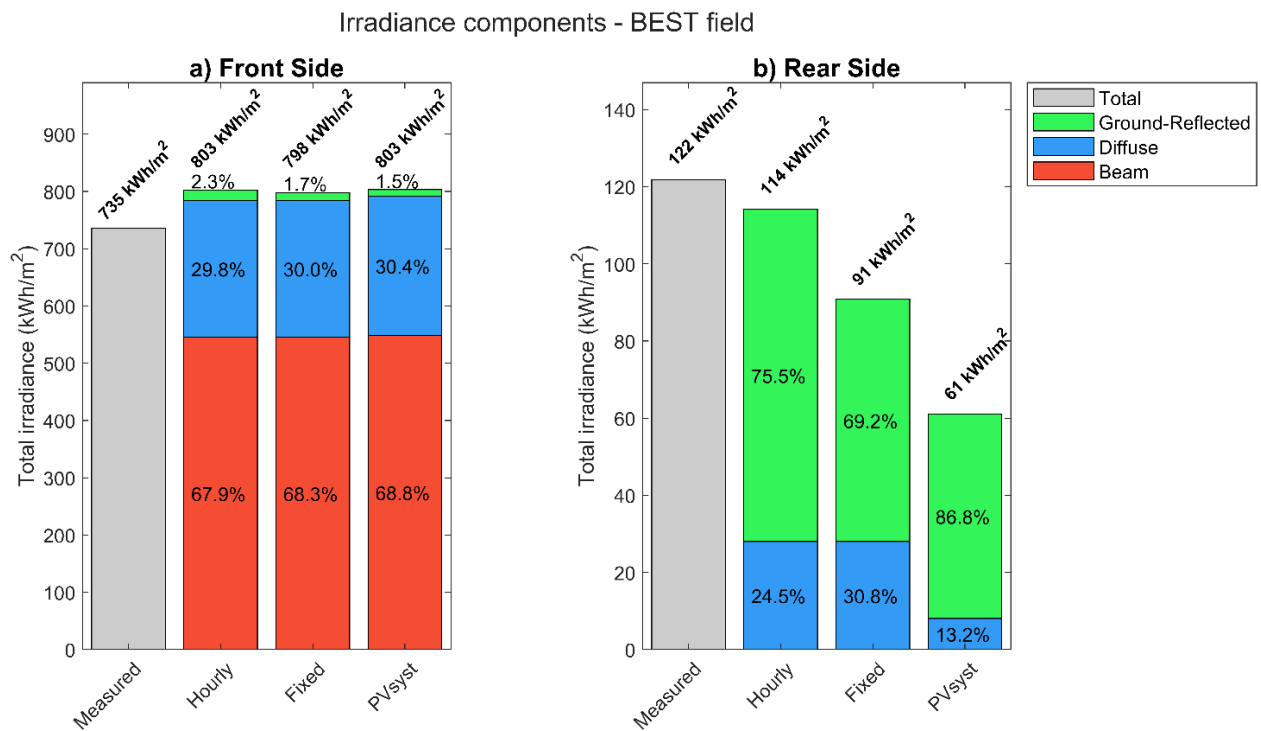


Figure 25 Irradiance components on the a) front and b) rear side of the results from the developed model with hourly and fixed albedo and PVsyst compared to the measured irradiance – NREL BEST field, for Oct-Apr. (Note the different scale of the y-axis)

5.2 Albedo effect on the irradiance: NREL BEST-field

Figure 26 shows scatterplots of the simulated irradiance at the NREL Bifacial Experimental Single-Axis Tracker field to the measured irradiance for October-November 2019 and April-March 2020, with hourly satellite-derived albedo and fixed albedo. The figure shows that an hourly changed albedo, a fixed albedo and a satellite-derived albedo gave a similar result when simulating the front side. The developed model was more accurate with an hourly albedo than the other two albedo alternatives.

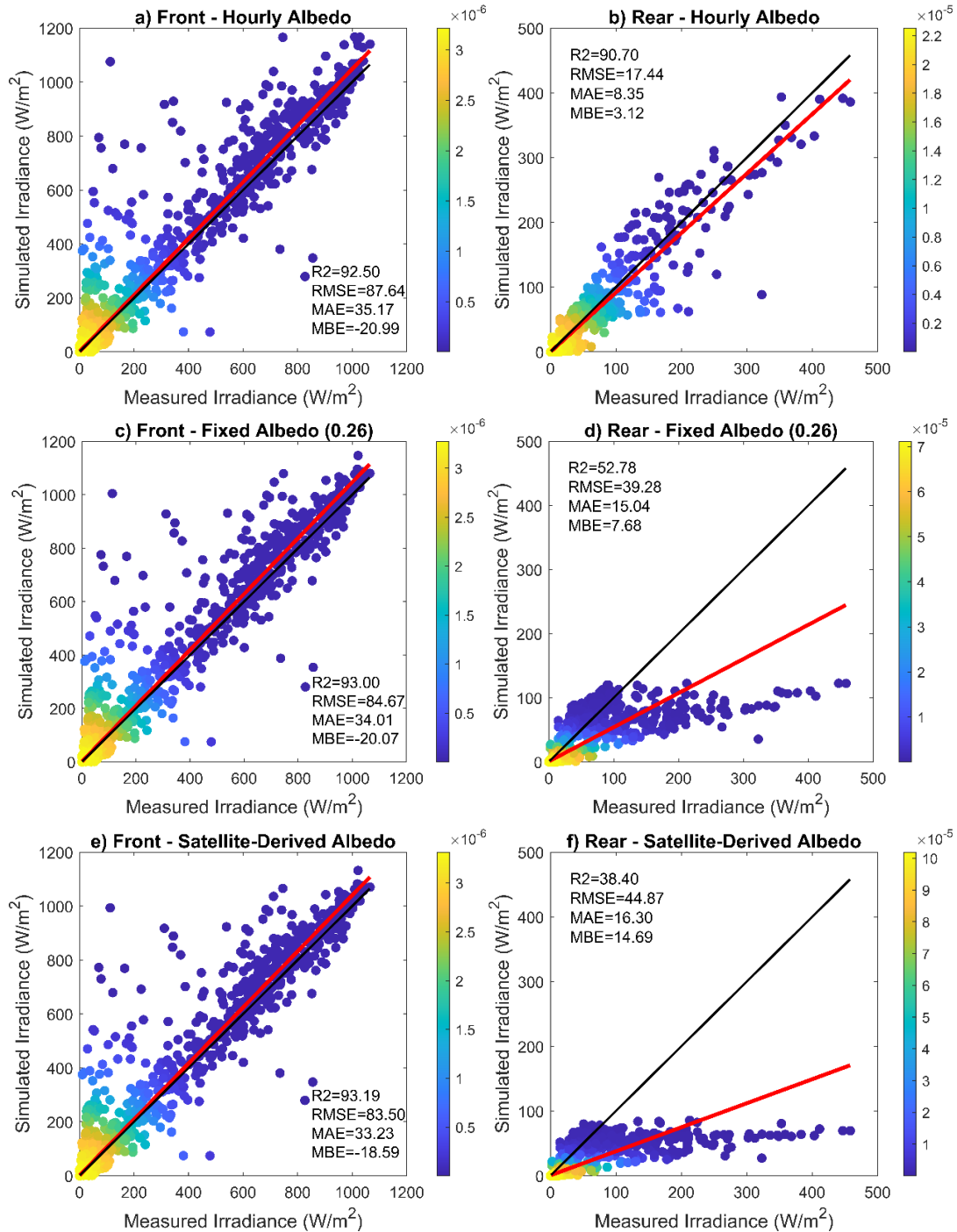


Figure 26 Scatterplots of the simulated result of front and rear irradiance with hourly (a-b), fixed (c-d) and satellite-derived (e-f) albedo - NREL BEST field, for Oct-Nov & Apr-Mar. The red line is a regression line, and the black line is an identity line. (Note the different scale of the y-axis)

The colour bar to the right in Figure 26 represents the data's density, where yellow means that the number of data points is high. The performance metrics for the simulations are summarised in Table 10.

Table 10 Comparison of performance metrics for hourly, fixed and satellite-derived albedo – NREL BEST field, Oct-Nov & Apr-Mar.

	Front				Rear			
	R2 (%)	RMSE (W/m ²)	MAE (W/m ²)	MBE (W/m ²)	R2 (%)	RMSE (W/m ²)	MAE (W/m ²)	MBE (W/m ²)
<i>Hourly</i>	92.50	87.64	35.18	-20.98	90.70	17.44	8.36	3.13
<i>Fixed (0.26)</i>	93.00	84.67	34.01	-20.07	52.78	39.28	15.04	7.68
<i>Satellite-derived</i>	93.19	83.50	33.23	-18.59	38.40	44.87	16.30	14.69

Figure 27 shows scatterplots of results from the developed model with various fixed albedo values. The figure illustrates that different fixed value does not reach as high accuracy, as the hourly albedo, for simulating the rear side irradiance of the single-axis tracker. The performance metrics for the simulations are summarised in Table 11.

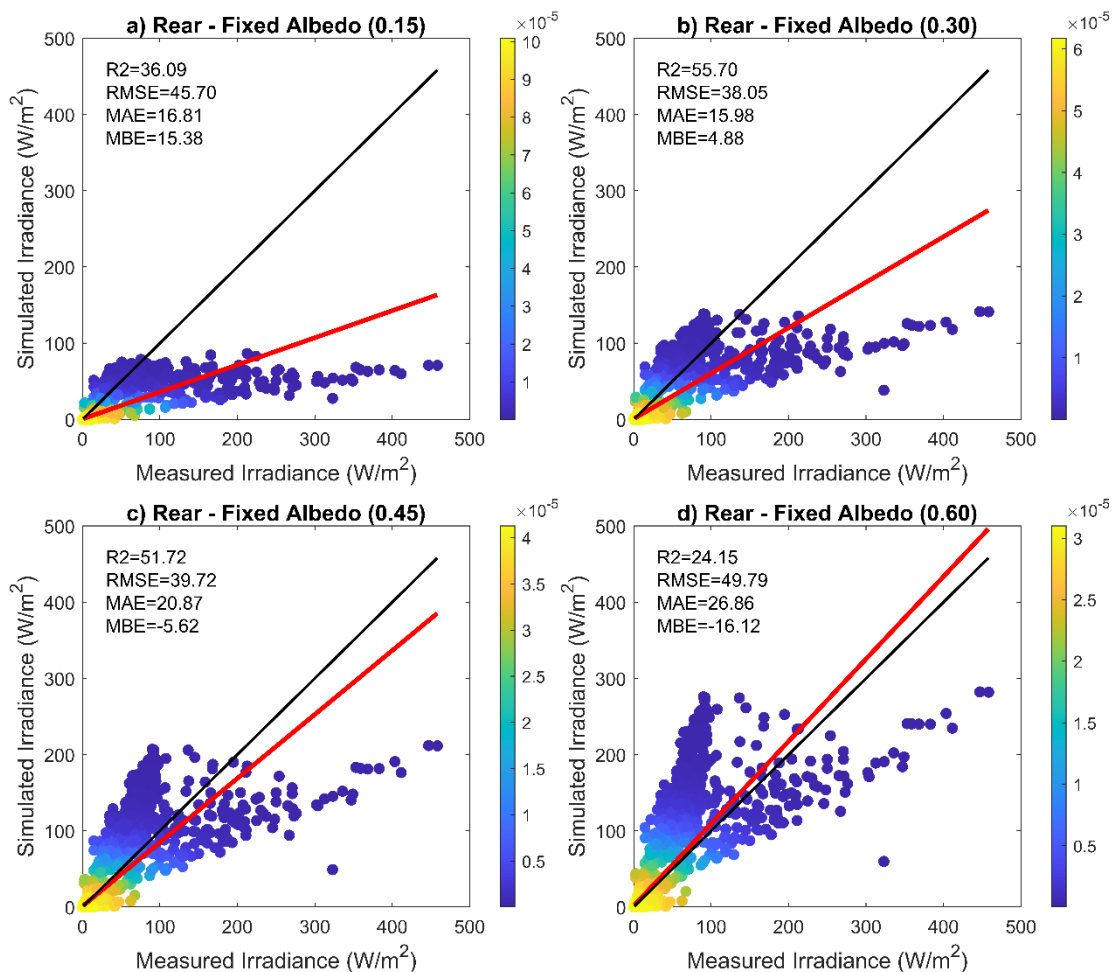


Figure 27 Scatterplots of the simulated result of rear irradiance with a fixed albedo of a) 0.15, b) 0.30, c) 0.45 and d) 0.60 - NREL BEST field, for Oct-Nov & Apr-Mar. The red line is a regression line, and the black line is an identity line. (Note the different scale of the y-axis)

Table 11 Comparison of performance metrics for a fixed albedo of 0.15, 0.30, 0.45 and 0.6 – NREL BEST field, Oct-Nov & Apr-Mar.

Rear				
	R2 (%)	RMSE (W/m ²)	MAE (W/m ²)	MBE (W/m ²)
<i>Fixed (0.15)</i>	36.09	45.70	16.81	15.38
<i>Fixed (0.30)</i>	55.70	38.05	15.98	4.88
<i>Fixed (0.45)</i>	51.72	39.72	20.87	-5.62
<i>Fixed (0.60)</i>	24.15	49.79	26.86	-16.12

5.3 Optimisation results: Kärrobo Prästgård

The developed model was used to investigate what tilt and azimuth angles would maximise the energy output for Kärrobo Prästgård during 2020. The optimisation result for the two installed bifacial PV systems at the farm is presented in the first column of Table 12 and Table 13, with fixed and hourly albedo values, respectively. Both albedo alternatives gave similar tilt and azimuth angles for the vertical (VS) and reference (RS) system. The second column of the two tables is the simulation result from installed configurations at the site. The results show that maximising the energy output would increase the total energy output for the vertical and reference system by approximately 2.1% and 8.5%, respectively, compared to the installed configurations.

Table 12 Result of the optimisation and the installed configurations with fixed albedo (0.2) for 2020.

<i>Fixed albedo</i>	<i>Maximised energy output</i>		<i>Installed configurations</i>	
	VS	RS	VS	RS
<i>Front tilt angle (°)</i>	90	54	90	30
<i>Front azimuth angle (°)</i>	-66	-39	-90	0
<i>Energy output (kWh)</i>	25 012	11 912	24 489	10 993
<i>Specific energy yield* (kWh/kWp)</i>	1 097	1 006	1 074	928
<i>Tot energy output (kWh)</i>	36 924		35 483	
<i>Tot elec. shortage (kWh)</i>	92 061		91 830	
<i>Tot elec. surplus (kWh)</i>	11 609		9 937	
<i>Tot self-consumption (kWh)</i>	25 314		28 545	
<i>Tot bought elec. (SEK)</i>	49 586		49 513	
<i>Tot savings** (SEK)</i>	11 320		11 393	
<i>Tot sold elec. (SEK)</i>	10 562		9 082	

* Specific energy yield = Energy output / Installed capacity

** Total saving = Total bought electricity without PV systems – Total bought electricity with PV systems

Table 13 Result of the optimisation and the installed configurations with hourly albedo for 2020.

Hourly albedo	Maximised energy output		Installed configurations	
	VS	RS	VS	RS
Front tilt angle (°)	90	54	90	30
Front azimuth angle (°)	-66	-39	-90	0
Energy output (kWh)	25 201	11 965	24 678	11 025
Specific energy yield* (kWh/kWp)	1 105	1 011	1 082	931
Tot energy output (kWh)	37 166		35 704	
Tot elec. shortage (kWh)	91 962		91 748	
Tot elec. surplus (kWh)	11 752		10 076	
Tot self-consumption (kWh)	25 414		25 627	
Tot bought elec. (SEK)	49 555		49 488	
Tot savings** (SEK)	11 351		11 419	
Tot sold elec. (SEK)	10 683		9 200	

* Specific energy yield = Energy output / Installed capacity

** Total saving = Total bought electricity without PV systems – Total bought electricity with PV systems

Figure 28 and Figure 29 show the front and rear side irradiance components for the vertical and reference system, respectively. The two PV systems are simulated with the developed model with the installed configurations (IC) and optimal configurations (OPT). The optimal configurations are the tilt and azimuth angles from Table 12 and Table 13, which maximises the yearly energy output. According to the developed model, the rear side irradiance of the reference can be increased significantly with the optimal configurations compared to the installed configurations.

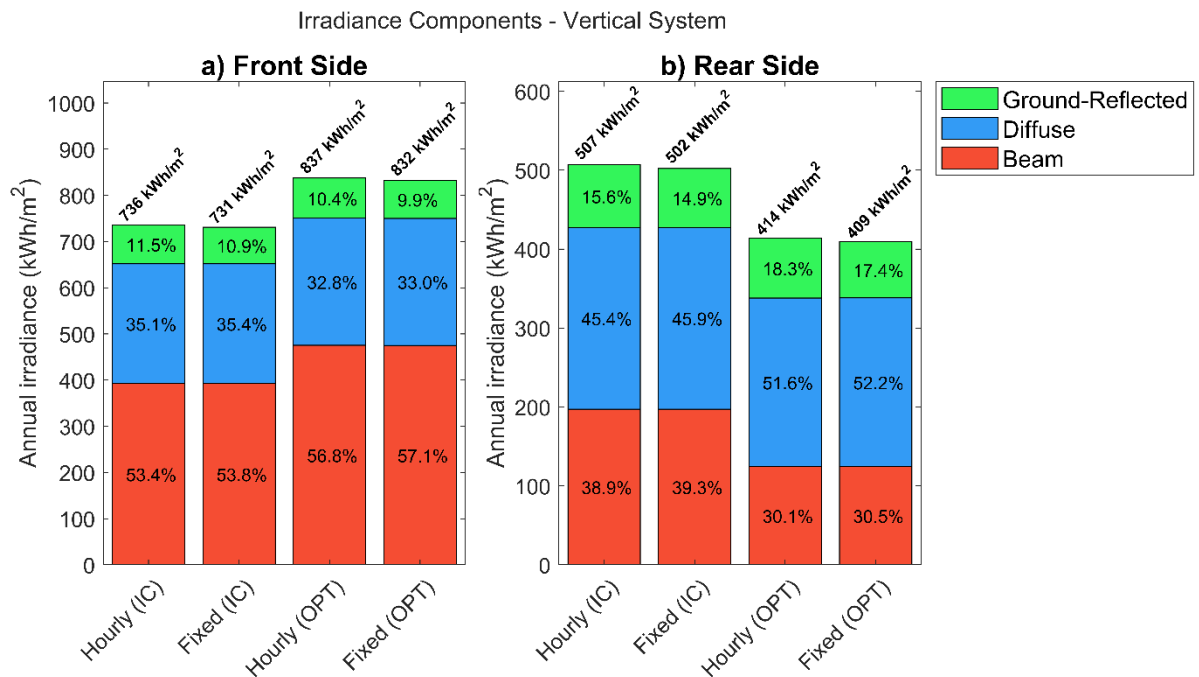


Figure 28 Irradiance components on the a) front and b) rear side of the vertical system with hourly and fixed albedo for optimal (OPT) and installed (IC) configurations – Kärrbo Prästgård, 2020. (Note the different scale of the y-axis)

Irradiance Components - Reference System

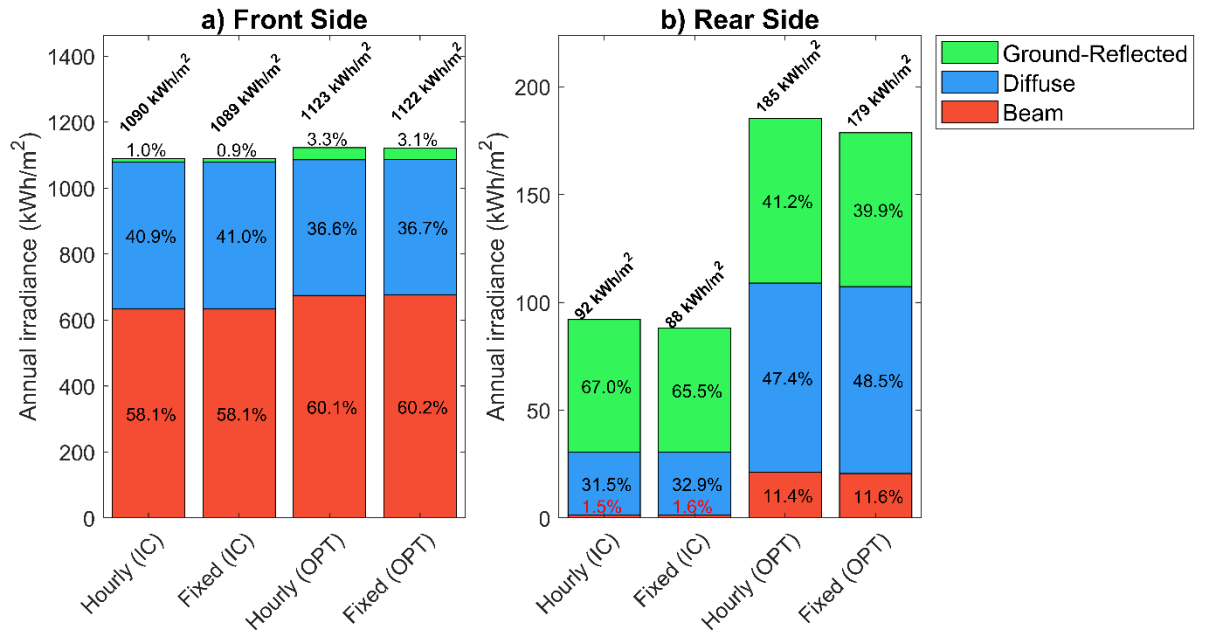


Figure 29 Irradiance components on the a) front and b) rear side of the reference system with hourly and fixed albedo for optimal (OPT) and installed (IC) configurations – Kärrbo Prästgård, 2020. (Note the different scale of the y-axis)

6 DISCUSSION

In this chapter, a discussion of the market price development of bifacial PV modules will be conducted based on the literature review. The second section will discuss the validation of the model and the effect on the simulation when using a dynamic or static albedo. Finally, the results from the optimisation will be analysed.

6.1 Market price development of bifacial PV

According to Fischer et al. (2021), the bifacial PV market is predicted to increase its market share of crystalline-silicon PV modules from 2020 and forward. The global market share of bifacial modules is forecasted to increase to 55% in 2031. IRENA (2020) reported that the global market price of PV modules had shown a significant decrease during the last ten years. The bifacial PV module price has since the year 2016 closed in on monofacial and high-performance monofacial modules. From 2018, bifacial and high-performance monofacial modules followed a similar price trend and closed in on the price of conventional monofacial modules. In 2019 a glass-back sheet monofacial PERC module of 375W had a 6% lower price per W_{DC} than a glass-glass bifacial PERC of 365W, according to Woodhouse et al. (2019). A similar price trend was shown on the European market between December 2019 and December 2020, according to Lusson (2020). The EU spot price of bifacial modules closed in on high performance and all-black modules.

Trends in Figure 5 and Figure 6 show that the price of bifacial modules decreases and may equalize the price of monofacial high-performance modules on a global scale. The decrease might be due to similar factors that affected the price of monofacial PV modules from 2009 until 2019. The growing market share of bifacial PV modules might be caused by increased bifacial PV manufacturers, leading to higher competition between bifacial PV manufacturers. It might also mean that already established bifacial PV manufacturers have increased their production of bifacial PV modules and benefitted from economies of scale. All of which might lead to decreasing prices.

6.2 Validation of model and evaluation of albedo

The results for the BEST field in Figure 24 show that the developed model generates similar accuracy as PVsyst for the front side. The coefficient of determination (R^2) is approximately 92 - 93 %. The other performance metrics show a similar result. While for the rear side, the developed model using hourly albedo succeeds the performance of PVsyst with a fixed albedo. Hourly albedo achieves an R^2 value of 91.44 for the rear side, while PVsyst achieves 42.33. PVsyst and the developed model, with fixed albedo, show similar accuracy when simulating the rear side irradiance of the BEST-field site. This result is consistent throughout the other performance metrics; The root mean square error (RMSE) is 15.47, 35.49, and 40.16 for hourly albedo, fixed albedo, and PVsyst, respectively. It is evident in Figure 24 f)

that PVsyst is not able to simulate the rear irradiance when the rear irradiance is higher than 120 W/m^2 due to hourly or daily peaks in the albedo value, seen in Figure 16.

Comparing different albedo values shows that the developed model generates more accurate results for the rear side when using hourly albedo than a fixed albedo. Further, the hourly albedo showed also better accuracy than the satellite-derived albedo. This result was consistent for simulating over the entire and albedo period. However, none of the two periods included time over the summer, which might have affected the result. From Figure 24, it is evident that the front side of the single-axis tracker was less affected than the rear side when simulating a bifacial PV with a dynamic or static albedo. One important note is that all the albedo alternatives had similar results for the front side and showed accurate results when comparing measured and simulated irradiance. The Copernicus satellite-derived albedo provided an albedo value covering a $1 \times 1 \text{ km}$ spatial resolution, a much larger area than the NREL BEST-field area. It might lead to the provided albedo for every tenth day depends on the surrounding infrastructure and environment. Therefore, the albedo should be measured at the site to decrease uncertainties caused by the surroundings. Which also Hutchins (2020a) and Marion (2021) pointed out. It should be noted that the front side of the single-axis tracker receives significantly more irradiance than the rear side. Thus, the total irradiance of the single-axis tracker is mainly affected by the front side simulations.

Since the model is a single-axis tracking system, the front side of the module will be highly impacted by direct and diffuse irradiance, as shown in Figure 25. At the same time, the rear side will be significantly affected by the diffuse irradiance and the albedo from the surroundings. Looking at Figure 16, it is likely that the BEST-field had snowfall and covered ground from time to time during the seven months of data, which might be the reasons for simulation overestimations shown in Figure 24. The overestimations of the front side could be caused by the front being covered by snow or soiling or any measurement error for irradiance input data as global and diffuse horizontal irradiance or the measured front irradiance. The rear irradiance with hourly albedo, in Figure 24, shows the tendency both to overestimate and underestimate the irradiation. The results are evenly distributed through the scatterplot, which affects the accuracy. Since the rear side of the single-axis tracker always points to the ground, it is probably less exposed to soiling and snow coverage than the front side. The developed model does not consider shading from the mounting structure, which could have affected the accuracy of the simulation result.

The albedo value also showed a tendency to be high in early and late hours of the day, impacted by angular and spectral effects, as Chiodetti et al. (2016), Zhang et al. (2012), and Iqbal (1983) stated. Hourly albedo values will record sudden increases or decreases in the albedo, as shown in Figure 17 and Figure 20, due to angular and spectral effects, snow- or rainfall. As Zhang et al. showed, the diurnal variations in albedo value form an up-facing parabolic curve. Due to uncertainties, a fixed albedo can have advantages compared to an hourly changing albedo in bifacial PV simulations. A fixed albedo will not depend on advanced measurement equipment and can be used in PVsyst or other validated bifacial PV simulation tools. The satellite-derived albedo can be retrieved free of charge but might, as the hourly albedo, not be applicable in developed simulation tools. The fixed albedo can then be considered more available and applicable than the dynamic albedo alternatives. However, in

this case, higher availability and applicability are not correlated with more accurate simulations of the irradiance on the rear side for the single-axis tracker due to the high share of ground-reflected irradiance. Chiodetti et al. (2016) agree that a variable albedo is more accurate than a static albedo. The evaluation of albedo value was limited to a few months during the winter season in Denver due to data availability. Thus, it has not included the result for summer season. The albedo value likely varies less during the summer than in the winter since there is no snow. However, seasonal changes of the surface are still to be expected. Suppose the study had evaluated the albedo values for the summer or an entire year. In that case, likely, the difference in rear side irradiance between hourly, satellite-derived, and fixed albedo would have been less significant.

This study was limited to evaluating how different albedos affect the simulation of bifacial PV modules. The hourly albedo used at the BEST-field was measured at the site and thus, as mentioned earlier, requires installment of advanced measurement equipment. Approaches for modelling the albedo values are based on the assumption that the albedo depends on the solar zenith angle (Dickinson, 1983; Briegleb et al., 1986). Although, modelling the black- and white-sky albedo requires an estimation or measurement of the albedo under direct illumination at solar zenith angle 60° (ρ_0) for equation (3) and (4). The ρ_0 value might be similar for every day for some surfaces, while some surfaces might have more significant variance since the value depends on the location, season and surface (Yang et al., 2008). Thus, modelling the albedo value might not be simple for all surfaces since it requires daily input. Chiodetti et al. (2016) state that the unknown parameters in equation (5), including the ρ_0 value, can be found by fitting the mathematical model towards measured data. This approach enables estimation of the albedo based on having advanced measurement equipment for a period. Thus, the availability of calculated albedo through the Chiodetti et al. approach can be regarded as more available. It should be noted that these equations have not been tested in the conducted study in this report.

There is a clear difference between the impact of albedo value for different PV systems. When comparing the ground-reflected irradiance for the single-axis tracker system (BEST field) in Figure 25 with the vertical and tilted system Kärro Prästgård, Figure 28 and Figure 29, it is evident that it differs. The front side of the single-axis tracker is not primarily affected by the ground-reflected irradiance, while the rear side is. The reference system shows a similar tendency as the single-axis tracker system; the rear side (both optimal and installed configuration) receives more ground-reflected irradiance than the front side. While for the vertical, both the front and rear sides have at least 10% of ground-reflected irradiance, indicating the importance of an accurate simulation of ground-reflected irradiance.

6.3 Optimal configurations of Kärro Prästgård

The optimisation to maximise the energy output of the vertical and reference PV system at Kärro Prästgård showed that using a static or dynamic albedo value does not affect the optimal configurations of the systems. The optimal tilt and azimuth angles were similar for both albedo simulations. The optimal configurations would have a minor increase in

electricity production for the vertical system of 2.1% than the installed configurations at Kärro Prästgård. In comparison, the reference system would increase electricity production by 8.5%. While the installed configurations would result in a minor electricity shortage than the optimal configuration, meaning that the farm would cover its electricity consumption to a more significant extent, which yields a lower total cost of bought electricity. The installed configurations would save about 70 SEK/year more in bought electricity than the optimal configuration. However, the optimal configurations would earn about 1 500 SEK/year more in selling electricity than the installed configurations. Thus, the income for optimal configurations is higher than the savings from installed configurations.

The mean value of the hourly albedo measured at Roskilde was 0.22 during the year, according to Marion (2020c), while the fixed albedo for simulations was 0.2. The hourly albedo, therefore, results in overall higher power output for both systems for any simulation. This result concurs with Sun et al. (2018) and Molin et al. (2018), who found that a higher albedo value increases the energy yield.

As shown earlier, the rear side of a single axis tracker irradiation is significantly affected by the albedo value since it only receives diffuse and ground-reflected irradiation (illustrated in Figure 25). While for a fixed tilted module, the rear side may, depending on the surroundings, receive direct irradiation at some point of the day, as shown in Figure 28 and Figure 29 for both installed systems at Kärro Prästgård. The overall trend in the figures shows that the significant irradiance component for the front side of the vertical and reference system is the direct beam and diffuse irradiance. While for the rear side, the irradiance components vary for both systems. The optimal configurations increase the rear side irradiance for all three irradiance components for the reference system. In contrast, the vertical systems show inconsistent results. The rear irradiance of the vertical system decreases when using optimal configurations, while the front irradiance increases. The shift is caused by the rear side irradiance being weighted by the bifaciality of the PV module (as seen in equation (42)), which favours the front side irradiance over the rear side irradiance.

There are limitations in the simulation tool, which might affect the result. The tool does not include any knowledge about the settings and surroundings of the PV systems at Kärro Prästgård, which neglects the shading of the surroundings and the row to row shading. The annual specific yield in Table 13 for the optimal vertical and the reference system was 1 105 kWh/kWp and 1 011 kWh/kWp, respectively, with an hourly changed albedo. These values should be regarded with caution since they are significantly higher than the specific yield reported by Molin et al. (2018) and Baumann et al. (2018). Zhang (2017b) mentioned that the specific yield depends on factors such as shading, which can have affected the simulation and overestimated the annual specific yield. Asgharzadeh et al. (2018) state that the optimal tilt depends on the albedo, elevation, size, weather condition and season. The same reasoning can be applied to the optimisation result from maximised energy for 2020 at Kärro Prästgård. Suppose the optimisation would have been performed for another year. In that case, the weather data would likely have affected the result and give other configurations that maximise the energy output.

Another uncertainty in the simulation is the albedo value. Due to the lack of hourly albedo for 2020 at Kärro Prästgård, the hourly albedo values used were measured at a grass surface located in Roskilde, Denmark. The distance between Roskilde and Kärro Prästgård is 517 km southwest of Kärro Prästgård. The hourly albedo values and the fixed albedo can only be used as estimations. Using an albedo for another location bring uncertainties with the results. Which is reinforced by the factors that Iqbal (1983) concluded affect the albedo value: sun position, solar spectrum, diffuse and beam irradiation, season and latitude. Due to the distance between Kärro Prästgård and Roskilde, the snowfall at Roskilde might not be applicable for Kärro Prästgård during 2020. Kärro Prästgård likely receives more snowfall than Roskilde due to being located further north. Snow may impact the vertical system differently than the reference system since the vertical system will be less affected by snow soiling than a lower tilted system, as Granlund et al. (2019) concluded. Also, snow on the ground may lead to increased albedo, as Chen et al. (2014) stated. Thus the uncertainty of the results may increase when snow is a factor present at the PV system site but not considered.

The economic computation is based on assumptions regarding the revenue of sold and bought electricity of 2020. It might not be applicable for the future as cost components of the electricity price change. The financial result was influenced by the spot prices of 2020, which was low compared to previous years (Rydegran, 2021). For the reference system, the optimal tilt angle differs by 24° compared to the installed configurations. However, the result does not include possible limitations concerning the installation cost and technology.

7 CONCLUSION

This study aimed to develop a model to simulate bifacial PV modules and assess how the albedo value impacts the performance. Furthermore, an optimisation of system configurations was conducted in addition to a price development review of bifacial PV modules. The main result shows that a mathematical model for bifacial PV modules has been developed to simulate both the received front and rear irradiance and energy output. Conclusions could be drawn that the developed model showed similar results to PVsyst when simulating the front side. The rear side showed more promising results simulating with the developed model and was more accurate than PVsyst when simulating the rear side irradiance. An hourly changed albedo was beneficial to use for more precise results than a fixed albedo. It was also evident when simulating with an hourly changing, a satellite-derived and a fixed albedo that the front and rear sides of the single-axis tracker bifacial module were affected differently. The front side of the single-axis tracker system did not significantly differ depending on the albedo alternative as the rear side. Thus, making the hourly changing albedo the best option. It can be concluded that the availability of measured albedo values at the location is essential in estimating the ground-reflected irradiance. The more detailed the dynamic albedo values, the more accurate simulations are achieved due to angular and spectral effects and seasonal changes.

The optimal configurations for the PV systems at Kärrobo Prästgård maximise the power output and minimize the electricity cost. The azimuth angle for the vertical bifacial PV system is -66° . While for a tilted reference system, the optimal tilt angle is 54° , and the azimuth angle is -39° . These optimal configurations would, in a year, save 11 300 SEK from self-consuming produced electricity and earn 10 600 SEK in selling electricity. However, the optimisation result should be regarded cautiously since the developed model is not validated against the systems at the farm. The literature study showed that the price of bifacial PV modules has decreased significantly and closed in on monofacial modules in the last five years. With a forecasted increase of bifacial PV market shares on the global market, competition and economies of scale may further decrease the price.

8 FURTHER STUDIES

This study shows that the front and rear irradiance on a single-axis tracker system can be simulated with the developed model. Further validation of the model to bifacial PV systems at other locations is necessary to ensure the models' accuracy. Also, the front side irradiance should be investigated further to validate and ensure that the outliers for the BEST field were due to snowfall or other measurement error. Further development of the developed model with row to row shading and shading from mounting structure would be essential to increase the models' accuracy.

Further studies in modelling the albedo value would be interesting to assess the importance and impact of albedo value to bifacial PV modules. The evaluation of albedo values highlighted the importance of a detailed dynamic albedo value in estimating the ground-reflected irradiance. It would be interesting to see the result of dynamic albedos in other developed simulation tools. Additionally, the dynamic albedo would be interesting to assess for different module elevation heights.

Due to the high specific yields of the two installed PV systems at Kärro Prästgård, validation of the model against the installed systems is necessary to ensure model accuracy. Further, optimising the system configurations at Kärro Prästgård with a dynamically measured albedo from the site would be valuable to evaluate the importance of the albedo value for optimisations.

9 REFERENCES

- AgriMetSoft. (2019). *Online Calculators*. Retrieved June 8, 2021, from agrimetsoft.com: <https://agrimetsoft.com/calculators/Mean%20Bias%20Error#>
- Appelbaum, J. (2016). Bifacial photovoltaic panels field. *Renewable Energy*, 85, 338-343. doi:<https://doi.org/10.1016/j.renene.2015.06.050>
- Appelbaum, J. (2018). The role of view factors in solar photovoltaic fields. *Renewable and Sustainable Energy Reviews*, 81, 161-171. doi:<https://doi.org/10.1016/j.rser.2017.07.026>
- Asgharzadeh, A., About Anoma, M., Hoffman, A., Chaudhari, C., Bapat, S., Perkins, R., . . . Bourne, B. (2019). A Benchmark and Validation of Bifacial PV Irradiance Models. *IEEE PVSC 46 Photovoltaic Specialists Conference (PVSC)* (pp. 3281-3287). Chicago, Illinois: IEEE. doi:<https://doi.org/10.1109/PVSC40753.2019.8981272>
- Asgharzadeh, A., Marion, B., Deline, C., Hansen, C., Stein, J. S., & Toor, F. (2018). A Sensitivity Study of the Impact of Installation Parameters and System Configuration on the Performance of Bifacial PV Arrays. *IEEE Journal of Photovoltaics*, 8(3), 798-805. doi:<https://doi.org/10.1109/JPHOTOV.2018.2819676>
- Ayala, S., & Deline, C. (2020a, June 9). *BEST_Data.csv*. Retrieved April 11, 2021, from datahub.duramat.org: <https://datahub.duramat.org/dataset/best-field-data/resource/1c3ac2d9-4734-49b5-b1e7-577a4cc62d80>
- Ayala, S., & Deline, C. (2020b, June 9). *NREL Bifacial Experimental Single-Axis Tracking Field*. Retrieved April 11, 2021, from datahub.duramat.org: <https://datahub.duramat.org/dataset/best-field-data/resource/dc5766d5-f62f-4716-a08b-of2c7f848a40> Reprinted with permission.
- Baumann, T., Carigiet, F., Knecht, R., Klenk, M., Dreisiebner, A., Nussbaumer, H., & Baumgartner, F. (2018). Performance Analysis of Vertically Mounted Bifacial PV Modules on Green Roof System. *35th European Photovoltaic Solar Energy Conference and Exhibition, Brussels, Belgium, September 24-28, 2018*. (pp. 1504-1509). Red Hook, NY: Curran Associates, Inc. doi:10.4229/35thEUPVSEC20182018-6AO.9.4
- Beasley, D., Bull, D. R., & Martin, R. R. (1993). An Overview of Genetic Algorithms: Part 1, Fundamentals. *University Computing*, 15(2), 58-69.
- Bellini, E. (2017, December 8). Longi claims 82.15% bifaciality record for its PERC solar cell. *pv magazine*. Retrieved May 11, 2021, from <https://www.pv-magazine.com/2017/12/08/longi-claims-82-15-bifaciality-record-for-its-perc-solar-cell/>
- Bellini, E. (2019, April 8). Imec, Jolywood announce 23.2% front-side conversion efficiency for n-PERT bifacial cell. *pv magazine*. Retrieved May 11, 2021, from <https://www.pv->

magazine.com/2019/04/08/imec-jolywood-announce-23-2-front-side-conversion-efficiency-for-n-pert-bifacial-cell/

- Briegleb, B. P., Minnis, P., Ramanathan, V., & Harrison, E. (1986). Comparison of Regional Clear-Sky Albedos Inferred from Satellite Observations and Model Computations. *Journal of Applied Meteorology and Climatology*, 25(2), 214-226. doi:[https://doi.org/10.1175/1520-0450\(1986\)025<0214:CORCSA>2.0.CO;2](https://doi.org/10.1175/1520-0450(1986)025<0214:CORCSA>2.0.CO;2)
- Campana, P. E., Holmberg, A., Pettersson, O., Klintonberg, P., Hangula, A., Benavente-Araoz, F., . . . Yan, J. (2016). An open-source optimization tool for solar home systems: A case study in Namibia. *Energy Conversion and Management*, 130, 106-118. doi:<https://doi.org/10.1016/j.enconman.2016.10.003>
- Campana, P. E., Li, H., Zhang, J., Zhang, R., Liu, J., & Yan, J. (2015). Economic optimization of photovoltaic water pumping systems for irrigation. *Energy Conversion and Management*, 95, 32-41. doi:<https://doi.org/10.1016/j.enconman.2015.01.066>
- Campana, P. E., Wästhage, L., Nookuea, W., Tan, Y., & Yan, J. (2019). Optimization and assessment of floating and floating-tracking PV systems integrated in on- and off-grid hybrid energy systems. *Solar Energy*, 177, 782-795. doi:<https://doi.org/10.1016/j.solener.2018.11.045>
- Campana, P. E., Zhang, Y., Lundblad, A., Li, H., & Jinyue, Y. (2017). An Open-source Platform for Simulation and Optimization of Clean Energy Technologies. *Energy Procedia*, 105, 946-952. doi:<https://doi.org/10.1016/j.egypro.2017.03.423>
- Cengel, Y. (2002). *Heat Transfer - A Practical Approach* (2nd ed.). McGraw-Hill, New York: McGraw-Hill Science, Engineering & Mathematics.
- Chen, A., Li, W., Li, W., & Liu, X. (2014). An observational study of snow aging and the seasonal variation of snow albedo by using data from Col de Porte, France. *Chinese Science Bulletin*, 59(34), 4881-4889. doi:<https://doi.org/10.1007/s11434-014-0429-9>
- Chioldetti, M., Lindsay, A., Dueyrat, P., Binesti, D., Luton, E., Radouane, K., & Mousel, S. (2016). PV Bifacial Yield Simulation with a Variable Albedo Model. *32nd European Photovoltaic Solar Energy Conference and Exhibition* (pp. 1449-1455). München: WIP Wirtschaft und Infrastruktur GmbH & Co Planungs KG. doi:<https://doi.org/10.4229/EUPVSEC20162016-5DP.1.4>
- Chowdhury, S., Quddammah Khokhar, M., Lee, S., Kim, Y., Park, J., Phong Pham, D., & Yi, J. (2021). p-type Heterojunction Bifacial Solar Cell with Rear Side Carrier Selective Contact. *Inorganic Chemistry Communications*, 108658. doi:<https://doi.org/10.1016/j.inoche.2021.108658>
- Climatedata. (n.d.). *Albedo*. Retrieved May 9, 2021, from Climate data information: <http://www.climatedata.info/forcing/albedo/>
- Collins. (2021). *Definition of 'bankable'*. Retrieved February 18, 2021, from collinsdictionary: <https://www.collinsdictionary.com/dictionary/english/bankable>

- Copernicus. (n.d.a). *Copernicus in detail*. Retrieved April 2, 2021, from copernicus.eu: <https://www.copernicus.eu/en/about-copernicus/copernicus-detail>
- Copernicus. (n.d.b). *Copernicus Global Land Service*. Retrieved April 2, 2021, from land.copernicus.eu: <https://land.copernicus.eu/global/products/sa>
- Cuevas, A., Luque, A., Eguren, J., & del Alamo, J. (1982). 50 Per cent more output power from an albedo-collecting flat panel using bifacial solar cells. *Solar Energy*, 29(5), 419-420. doi:[https://doi.org/10.1016/0038-092X\(82\)90078-0](https://doi.org/10.1016/0038-092X(82)90078-0)
- Deline, C., MacApline, S., Marion, B., Toor, F., Asgharzadeh, A., & Stein, J. S. (2017). Assessment of Bifacial Photovoltaic Module Power Rating Methodologies—Inside and Out. *IEEE Journal of Photovoltaics*, 7(2), 575-580. doi:<https://doi.org/10.1109/JPHOTOV.2017.2650565>
- Dickinson, R. E. (1983). Land Surface Processes and Climate - Surface Albedos and Energy Balance. *Advances in Geophysics*, 25, 305-353. doi:[https://doi.org/10.1016/S0065-2687\(08\)60176-4](https://doi.org/10.1016/S0065-2687(08)60176-4)
- Duffie, J., & Beckman, W. (2006). *Solar Engineering of Thermal Processes*. Hoboken, New Jersey: John Wiley & Sons, Inc.
- Dullweber, T., Kranz, C., Peibst, R., Baumann, U., Hannebauer, H., Fülle, A., . . . Neuhaus, D. H. (2015). PERC+: industrial PERC solar cells with rear Al grid enabling bifaciality and reduced Al paste consumption. *Proceedings of the 31st European Photovoltaic Solar Energy Conference*, 341-350. doi:<https://doi.org/10.1002/pip.2712> Reprinted with permission.
- Energimarknadsbyrån. (2020a, March 10). *Solcellskalkyl och prisutveckling*. Retrieved April 10, 2021, from energimarknadsbyran.se: <https://www.energimarknadsbyran.se/solceller/kopa-solceller-och-salja-solel/ar-solceller-for-villa-lonsamt/solcellskalkyl-och-prisutveckling/>
- Energimarknadsbyrån. (2020b, March 10). *Skattereduktion och skattebefrielse*. Retrieved June 9, 2021, from energimarknadsbyran.se: <https://www.energimarknadsbyran.se/solceller-2/skattereduktion-och-skattebefrielse/>
- EnergyPal. (n.d). *Jolywood Sunwatt JW-D72N-380 Series (Multi-Busbar Full Frame)*. Retrieved May 4, 2021, from cdn.energypal: https://cdn.energypal.com/panels/jw-d72n-380/energypal-solar-panel-spec-datasheet-jolywood-sunwatt-jw-d72n-series-multi-busbar-full-frame-jw-d72n-380.pdf?_gl=1*1bc8ono*_ga*YW1wLVZHMEExZSmxnREpQX1gyTWZyTUEExTHc
- EnergyPlus. (n.d.). *Climate, Sky and Solar/Shading Calculations*. Retrieved April 10, 2021, from eneryplus.net: https://www.energyplus.net/sites/default/files/docs/site_v8.3.0/EngineeringReference/05-Climate/index.html

- Fischer, M., Woodhouse, M., Herritsch, S., & Trube, J. (2021). *International Technology Roadmap for Photovoltaic (ITRPV) 2020 Results*. Frankfurt am Main: VDMA photovoltaic Equipment.
- FOREX. (2021, April 21). *USA-DOLLAR - USD*. Retrieved April 21, 2021, from forex.se: <https://www.forex.se/valuta/usd>
- Glen, S. (n.d.). *Coefficient of determination (R squared): Definition, Calculation*. Retrieved June 7, 2021, from StatisticsHowTo.com: Elementary Statistics for the rest of us!: <https://www.statisticshowto.com/probability-and-statistics/coefficient-of-determination-r-squared/>
- Grace-Martin, K. (n.d.). *Assesing the Fit of Regression Models*. Retrieved June 8, 2021, from The analysis factor: <https://www.theanalysisfactor.com/assessing-the-fit-of-regression-models/>
- Granlund, A., Narvesjö, J., & Petersson, A. M. (2019). The Influence of Module Tilt on Snow Shadowing of Frameless Bifacial Modules. *36th European Photovoltaic Solar Energy Conference and Exhibition* (pp. 1650-1654). Marseille: RISE Energy Technology Center. doi:<https://doi.org/10.4229/EUPVSEC20192019-5CV.4.36>
- Grant, I. F., Prata, A. J., & Cechet, R. P. (2000). The Impact of the Diurnal Variation of Albedo on the Remote Sensing of the Daily Mean Albedo of Grassland. *Journal of Applied Meteorology and Climatology*, 39(2), 231-244. doi:[https://doi.org/10.1175/1520-0450\(2000\)039<0231:TIOTDV>2.0.CO;2](https://doi.org/10.1175/1520-0450(2000)039<0231:TIOTDV>2.0.CO;2)
- Gueymard, C. (2018). A reevaluation of the solar constant based on a 42-year total solar irradiance time series and a reconciliation of spaceborne observations. *Solar Energy*, 168, 2-9. doi:<https://doi.org/10.1016/j.solener.2018.04.001>
- Guillevin, N., Cesar, I., Burgers, A., Venema, P., Wang, Z., Zhai, J., & Liu, D. (2017). Pilot Line Results of n-Type IBC Cell Process in Mass Production Environment. *33rd European Photovoltaic Solar Energy Conference and Exhibition*, (pp. 201-211). Amsterdam. doi:<https://doi.org/10.4229/EUPVSEC20172017-2BP.1.2>
- Guo, S., Walsh, T. M., & Peters, M. (2013). Vertically mounted bifacial photovoltaic modules: A global analysis. *Energy*, 61, 447-454. doi:<https://doi.org/10.1016/j.energy.2013.08.040>
- Hajjar, H. K., Dubaikel, F. A., & Ballard, I. (2015). Bifacial photovoltaic technology for the oil and gas industry. *2015 Saudi Arabia Smart Grid Conference (SASG)*, 1-4. doi:<https://doi.org/10.1109/SASG.2015.7449283>.
- Hooper, F. C., & Brunger, A. P. (1980). A model for the angular distribution of sky radiance. *Journal of Solar Energy Engineering*, 102(3), 196-202. doi:<https://doi.org/10.1115/1.3266154>
- Hu, D., Zhang, S., Lian, W., Wang, J., Ni, Z., & Wei, Q. (2019). Efficiency improvement of bifacial PERC solar cell based on the optimization of rear surface. *AIP Conference*

- Proceedings 2147* (p. 110003). AIP Publishing.
doi:<https://doi.org/10.1063/1.5123879>
- Hutchins, M. (2020a, January 25). The long read: All about albedo. *pv magazine*. Retrieved May 2, 2021, from <https://www.pv-magazine-india.com/2020/01/25/the-long-read-all-about-albedo/>
- Hutchins, M. (2020b, January 31). Perovskite/silicon tandem solar cells approaching 30% efficiency in lab. *pv magazine*. Retrieved May 10, 2021, from <https://pv-magazine-usa.com/2020/01/31/tandem-cells-approaching-30-efficiency/>
- IEA. (2019). *Renewables 2019 - Analysis and forecasts to 2024*. IEA Publications. Retrieved from webstore.iea.org/renewables-2019
- Iqbal, M. (1983). *An Introduction To Solar Radiation*. Academic Press.
- IRENA. (2020). *Renewable Power Generation Costs in 2019*. Abu Dhabi: International Renewable Energy Agency.
- Kasten, F., & Young, A. (1989). Revised optical air mass tables and approximation formula. *Applied Optics*, 28(22), 4735-4738. doi:<https://doi.org/10.1364/ao.28.004735>
- Katsaounis, T., Kotsovos, K., Gereige, I., Basaheeh, A., Abdullah, M., Khayat, A., . . . Tzavaras, A. (2019). Performance assessment of bifacial c-Si PV modules through device simulations and outdoor measurements. *Renewable Energy*, 143, 1285-1298. doi:<https://doi.org/10.1016/j.renene.2019.05.057>
- Kéry, M., & Royle, J. A. (2016). Chapter 10 - Modeling Static Occurrence and Species Distributions Using Site-occupancy Models. In M. Kéry, & J. A. Royle, *Applied Hierarchical Modeling in Ecology: Analysis of Distribution, Abundance and Species Richness in R and BUGS: Volume 1: Prelude and Static Models* (pp. 551-629). Elsevier Inc. doi:<http://dx.doi.org/10.1016/B978-0-12-801378-6.00010-2>
- Khan, R., Hanna, A., Sun, X., & Alam, M. (2017). Vertical bifacial solar farms: Physics, design, and global optimization. *Applied Energy*, 206, 240-248. doi:<https://doi.org/10.1016/j.apenergy.2017.08.042>
- Lave, M. S. (2015). *Albedo and Diffuse POA Measurements to Evaluate Transposition Model Uncertainty*. Livermore: Sandia National Laboratories. doi:<https://doi.org/10.2172/1529054>
- Lee, T., & Ebong, A. (2017). A review of thin film solar cell technologies and challenges. *Renewable and Sustainable Energy Reviews*, 70, 1286-1297. doi:<https://doi.org/10.1016/j.rser.2016.12.028>
- Lehr, J., Langenhorst, M., Schmager, R., Gota, F., Kirner, S., Lemmer, U., . . . Paetzold, U. W. (2020). Energy yield of bifacial textured perovskite/silicon tandem photovoltaic modules. *Solar Energy Materials and Solar Cells*, 208, 110367. doi:<https://doi.org/10.1016/j.solmat.2019.110367>

- Lellouch, G., Carrer, D., Vincent, C., Pardé, M., Frietas, S. C., & Trigo, I. F. (2020). Evaluation of Two Global Land Surface ALbedo Datasets Distributed by the Copernicus Climate Change Service and the EUMETSAT LSA-SAF. *Remote Sensing*, *12*(11), 1888. doi:<https://doi.org/10.3390/rs12111888>
- Leloux, J., Taylor, J., Moretón, R., Narvarte, L., Trebosc, D., & Desportes, A. (2015). Monitoring 30,000 PV systems in Europe: Performance, Faults, and State of the Art. *31st European Photovoltaic Solar Energy Conference and Exhibition, Hamburg, Germany, September 14-18, 2015*. (pp. 1574-1582). Red Hook, NY: Curran Associates, Inc. doi:10.4229/EUPVSEC20152015-5AO.8.1
- Lewis, P., & Barnsley, M. J. (1994). Influence of the Sky Radiance Distribution on Various Formulations of the Earth Surface Albedo. *Proceedings of the International Symposium on Physical Measurements and Signatures in Remote Sensing*, 17-21.
- Li, H., & Zhang, W. (2020). Perovskite Tandem Solar Cells: From Fundamentals to Commercial Deployment. *Chemical Reviews*, *120*, 9835-9950. doi:<https://doi.org/10.1021/acs.chemrev.9b00780>
- Liang, T. S., Pravettoni, M., Deline, C., Stein, J. S., Kopecek, R., Singh, J. P., . . . Sheng Khoo, Y. (2019). A review of crystalline silicon bifacial photovoltaic performance characterisation and simulation. *Energy & Environmental Science*, *12*, 116-148. doi:<https://doi.org/10.1039/c8ee02184h>
- Liang, T. S., Pravettoni, M., Singh, J. P., Wang, Y., & Khoo, Y. S. (2018). Towards IEC TS 60904-1-2: Assessing The Requirements for Irradiance on the Non-Illuminated Side of Bifacial Pv Modules With Single Light Source Testing. *35th European Photovoltaic Solar Energy Conference and Exhibition*, (pp. 1017-1023). Brussels. doi:<https://doi.org/10.4229/35thEUPVSEC20182018-5BO.10.1>.
- Lindsay, A., Chioldetti, M., Dupeyrat, P., Binesti, D., Lutun, E., & Radouane, K. (2015). Key Elements in the Design of Bifacial PV Power Plants. *31st European Photovoltaic Solar Energy Conference and Exhibition, Hamburg, Germany, September 14-18, 2015*. (pp. 1764-1769). Red Hook, NY: Curran Associates, Inc. doi:<https://doi.org/10.4229/EUPVSEC20152015-5CO.14.4>
- Lohmüller, E., Lohmüller, S., Norouzi, M., Mack, S., Demant, M., Gutscher, S., . . . Wol, A. (2017). Bifacial p-Type Silicon PERL Solar Cells with Screen-Printed Pure Silver Metallization and 89% Bifaciality. *33rd European PV Solar Energy Conference and Exhibition*, (pp. 418-423). Amsterdam. doi:<https://doi.org/10.4229/EUPVSEC20172017-2CO.11.3>
- LONGi Solar. (2020). *Hi-MO4 Bifacial and Monofacial Modules*. Retrieved May 4, 2021, from longi-solar: <https://www.longi-solar.com.au/uploads/attach/20201211/5fd3347dd2579.pdf>

- Lusson, N. (2020, August 19). Bifacial modules: The challenges and advantages. *pv magazine*. Retrieved April 26, 2021, from <https://www.pv-magazine.com/2020/08/19/bifacial-modules-the-challenges-and-advantages/>.
- Marion, B. (2020a, July 23). *RoskildeDenmark_Hourly.csv*. Retrieved May 14, 2021, from DuraMAT: https://datahub.duramat.org/dataset/cc19800f-33d7-4aae-b717-efffc2711613/resource/e850f974-420a-4a2d-b8e8-e75753f0d29e/download/roskildeddenmark_hourly.csv
- Marion, B. (2020b). Albedo Data Sets for Bifacial PV Systems. *47th IEEE Photovoltaic Specialists Conference (PVSC)* (pp. 485-489). Calgary: National Renewable Energy Laboratory. Retrieved from <http://ieeexplore.ieee.org/stamp/stamp.jsp?tp=&arnumber=9300470&isnumber=9300350>
- Marion, B. (2020c, July 23). *User's Guide for Albedo Data Sets Rev3.pdf*. Retrieved May 14, 2021, from DuraMAT: <https://datahub.duramat.org/dataset/d1c1fc62-eb76-477e-a07b-6bb0dc8e813c/resource/6206db10-c5b4-4635-a870-ec23efd1c181/download/users-guide-for-albedo-data-sets-rev3.pdf>
- Marion, B. (2021). Measured and satellite-derived albedo data for estimating bifacial photovoltaic system performance. *Solar Energy*, *215*, 321-327. doi:<https://doi.org/10.1016/j.solener.2020.12.050>
- Markvart, T., & Castañer, L. (2017). Semiconductor Materials and Modeling. In S. A. Kalogirou, *McEvoy's Handbook of Photovoltaics* (3rd ed., pp. 29-57). Academic Press. doi:<https://doi.org/10.1016/B978-0-12-809921-6.00002-1>
- Martín, N., & Ruiz, J. M. (2002). A new model for PV modules angular losses under field conditions. *International Journal of Solar Energy*, *22*(1), 19-31. doi:<https://doi.org/10.1080/01425910212852>
- Martín, N., & Ruiz, J. M. (2004). Annual angular reflection losses in PV modules. *Progress in Photovoltaics: Research and applications*, *13*(1), 75-84. doi:<https://doi.org/10.1002/pip.585>
- Masson, G., & Kaizuka, I. (2020). *Trends in photovoltaic applications 2020*. IEA PVPS. Retrieved from https://iea-pvps.org/wp-content/uploads/2020/11/IEA_PVPS_Trends_Report_2020-1.pdf
- Masters, G. M. (2004). *Renewable and Efficient Electric Power Systems*. Hoboken, New Jersey: John Wiley & Sons, Inc.
- Mathworks. (n.d.a). *Math. Graphics. Programming*. Retrieved February 18, 2021, from [se.mathworks.se: https://se.mathworks.com/products/matlab.html?s_tid=hp_products_matlab](https://se.mathworks.com/products/matlab.html?s_tid=hp_products_matlab)

- MathWorks. (n.d.b). *Get started with Optimization Toolbox*. Retrieved May 11, 2021, from se.mathworks.com: <https://se.mathworks.com/help/optim/getting-started-with-optimization-toolbox.html>
- Merei, G., Berger, C., & Saur, D. U. (2013). Optimization of an off-grid hybrid PV-Wind-Diesel system with different battery technologies using genetic algorithm. *Solar Energy*, 97, 460-473. doi:<https://doi.org/10.1016/j.solener.2013.08.016>
- Mermoud, A., & Wittmer, B. (2016, 10 25). *Bifacial shed simulations with PVsyst*. Retrieved May 2, 2021, from npv-workshop.com: http://npv-workshop.com/fileadmin/layout/images/Konstanz-2017/2__B._Wittmer_PV_SYST_Bifacial_shed_simulations.pdf
- Mihailetchi, V., Chu, H., Galbiati, G., Comparroto, C., Halm, A., & Kopecek, R. (2015). A comparison study of n-type PERT and IBC cell concepts with screen printed contacts. *5th International Conference on Silicon Photovoltaics, SiliconPV 2015* (pp. 534-539). Konstana: Elsevier Ltd. doi:<https://doi.org/10.1016/j.egypro.2015.07.076>
- Molin, E., Stridh, B., Molin, A., & Wäckelgård, E. (2018). Experimental Yield Study of Bifacial PV Modules in Nordic Conditions. *IEEE Journal of Photovoltaics*, 8(6), 1457-1463. doi:<https://doi.org/10.1109/JPHOTOV.2018.2865168>
- National Snow & Ice Data Center. (2020). *Thermodynamics: Albedo*. Retrieved January 26, 2021, from National Snow & Ice Data Center: <https://nsidc.org/cryosphere/seaice/processes/albedo.html>
- Nord Pool. (2021, January 01). *Historical Market Data. Elspot Prices_2020_Monthly_SEK*. Retrieved April 22, 2021, from nordpoolgroup.com: <https://www.nordpoolgroup.com/historical-market-data/>
- NREL. (n.d.a). *Solar Photovoltaic Technology Basics*. Retrieved May 10, 2021, from nrel.gov: <https://www.nrel.gov/research/re-photovoltaics.html>
- NREL. (n.d.b). *Best Research-Cell Efficiency Chart*. Retrieved May 10, 2021, from nrel.gov: <https://www.nrel.gov/pv/cell-efficiency.html>
- OptiCE. (n.d.). *Home*. Retrieved February 10, 2021, from optice.net: <http://optice.net/index.html>
- Patel, M. T., Khan, M. R., Sun, X., & Alam, M. A. (2019). A worldwide cost-based design and optimization of tilted bifacial solar farms. *Applied Energy*, 247, 467-479. doi:<https://doi.org/10.1016/j.apenergy.2019.03.150>
- Perez, R., Ineichen, P., Seals, R., Michalsky, J., & Stewart, R. (1990). Modeling daylight availability and irradiance components from direct and global irradiance. *Solar Energy*, 44(5), 271-289. doi:[https://doi.org/10.1016/0038-092X\(90\)90055-H](https://doi.org/10.1016/0038-092X(90)90055-H)

- Perez, R., Stewart, R., Seals, R., & Guertin, T. (1988). *The Development and Verification of the Perez Diffuse Radiation Model*. Albuquerque: Sandia National Laboratories. doi:<https://doi.org/10.2172/7024029>
- Phillips, A., Khanal Subedi, K., Liyanage, G., Alfadhili, F., Ellingson, R., & Heben, M. (2020). Understanding and Advancing Bifacial Thin Film Solar Cells. *ACS Applied Energy Materials*, 6072-6078. doi:<https://doi.org/10.1021/acsaem.0c00851>
- PVinfoLink. (n.d.). *InfoLink*. Retrieved February 10, 2021, from [infolink-group.com/en](http://www.infolink-group.com/en): <https://www.infolink-group.com/en>
- PVPMC Sandia. (n.d.). *PV_LIB Toolbox for Matlab Function Documentation and Help*. Retrieved May 5, 2021, from PVPerformance Modeling Collaborative: https://pvpmc.sandia.gov/PVLIB_Matlab_Help/
- PVsystem. (n.d.a). *Bifacial Systems*. Retrieved May 3, 2021, from [pvsystem.com](http://www.pvsystem.com): https://www.pvsystem.com/help/bifacial_systems.htm
- PVsystem. (n.d.b). *Albedo coefficient*. Retrieved May 3, 2021, from [pvsystem.com](http://www.pvsystem.com): <https://www.pvsystem.com/help/albedo.htm>
- PVsystem. (n.d.c). *About Us*. Retrieved May 9, 2021, from [pvsystem.com](http://www.pvsystem.com): <https://www.pvsystem.com/about-us/>
- pvXchange. (2020, December 14). Retrieved April 7, 2021, from [pvXchange.com](http://www.pvxchange.com): <https://www.pvxchange.com/>
- Renner, G., & Ekárt, A. (2003). Genetic algorithms in computer aided design. *Computer-Aided Design*, 35(8), 709-726. doi:[https://doi.org/10.1016/S0010-4485\(03\)00003-4](https://doi.org/10.1016/S0010-4485(03)00003-4)
- Rodríguez-Gallegos, C., Bieri, M., Gandhi, O., Singh, J. P., Reindl, T., & Panda, S. K. (2018). Monofacial vs bifacial Si-based PV modules: Which one is more cost-effective? *Solar Energy*, 176, 412-438. doi:<https://doi.org/10.1016/j.solener.2018.10.012>
- Rydegran, E. (2021, February 9). *Rekordlåga elpriser sammanfattar elåret 2020*. Retrieved June 9, 2021, from [energiforetagen.se](http://www.energiforetagen.se): <https://www.energiforetagen.se/pressrum/pressmeddelanden/2020/rekordlaga-elpriser-sammanfattar-elaret-2020/>
- Schachinger, M. (2021, January 20). Module Price Index: 2020 - Taking the time to say 'thanks'... *pv magazine*. Retrieved April 17, 2021, from <https://www.pv-magazine.com/2021/01/20/module-price-index-2020-taking-the-time-to-say-thanks/> Reprinted with permission.
- Schelin, E. (2019). *Photovoltaic System Yield Evaluation in Sweden: A performance review of PV systems in Sweden 2017-2018*. (Master's thesis, Mälardalen University, Västerås). Retrieved from <http://urn.kb.se/resolve?urn=urn:nbn:se:mdh:diva-44667>

- Shaw, J. A., & Vollmer, M. (2017). Blue sun reflected from water: optical lessons from observations of nature. *Proceedings Volume 10452, 14th Conference on Education and Training in Optics and Photonics, ETOP 2017, Hangzhou, China, August 16, 2017*. SPIE. doi:<https://doi.org/10.1117/12.2270481>
- Shoukry, I., Libal, J., Kopecek, R., Wefringhaus, E., & Werner, J. (2016). Modelling of Bifacial Gain for Stand-alone and in-field Installed Bifacial PV Modules. *Energy Procedia*, 92, 600-608. doi:<https://doi.org/10.1016/j.egypro.2016.07.025>
- Singh, J. P., Gou, S., Peters, I. M., Aberle, A. G., & Walsh, T. M. (2015). Comparison of Glass/Glass and Glass/Backsheet PV Modules Using Bifacial Silicon Solar Cells. *IEEE Journal of Photovoltaics*, 5(3), 783-791. doi:<https://doi.org/10.1109/JPHOTOV.2015.2405756>
- Skatteverket. (n.d.). *Energiskatter*. Retrieved 05 23, 2021, from [skatteverket.se: https://skatteverket.se/foretagochorganisationer/skatter/punktskatter/energiskatter.4.18e1b10334ebe8bc8000843.html](https://skatteverket.se/foretagochorganisationer/skatter/punktskatter/energiskatter.4.18e1b10334ebe8bc8000843.html)
- SMHI. (n.d.a). *Öppna data*. Retrieved February 17, 2020, from [smhi.se: https://www.smhi.se/data/oppna-data](https://www.smhi.se/data/oppna-data)
- SMHI. (n.d.b). *STRÅNG - en modell för solstrålning*. Retrieved February 17, 2021, from [smhi.se: https://www.smhi.se/forskning/forskningsenheter/atmosfarisk-fjarranalys/strang-en-modell-for-solstralning-1.329](https://www.smhi.se/forskning/forskningsenheter/atmosfarisk-fjarranalys/strang-en-modell-for-solstralning-1.329)
- Sreenath, S., Sudhakar, K., & Yusop, A. F. (2021). Performance assessment of conceptual bifacial solar PV system in varying albedo conditions. *IOP Conference Series: Materials Science and Engineering*. 1078, p. 012033. Pekan: IOP Publishing. doi:<https://doi.org/10.1088/1757-899X/1078/1/012033>
- Stein, J., Holmgren, W., Forbess, J., & Hansen, C. (2016). PVLIB: Open Source Photovoltaic Performance Modeling Functions for Matlab and Python. *2016 IEEE 43rd Photovoltaic Specialists Conference (PVSC), Portland, Oregon, USA, June 5-10, 2016*. (pp. 3425-3430). Red Hook, NY: Curran Associates, Inc. doi:<https://doi.org/10.1109/PVSC.2016.7750303>
- Stein, J., Reise, C., Bonilla Castro, J., Friesen, G., Magueri, G., Urrejola, E., & Ranta, S. (2021). *Bifacial Photovoltaic Modules and Systems: Experience and Results from International Reserach and Pilot Applications 2021*. IEA-PVPS. Retrieved from https://iea-pvps.org/wp-content/uploads/2021/04/IEA-PVPS-T13-14_2021-Bifacial-Photovoltaic-Modules-and-Systems-report.pdf
- Sun, X., Khan, M. R., Deline, C., & Alam, M. A. (2018). Optimization and performance of bifacial solar modules: A global perspective. *Applied Energy*, 212, 1601-1610. doi:<https://doi.org/10.1016/j.apenergy.2017.12.041>
- Sundaram, S., Benson, D., & Mallick, T. (2016). *Solar Photovoltaic Technology Production*. Penryn: Academic Press. doi:<https://doi.org/10.1016/B978-0-12-802953-4.00002-0>

- Teppe, A., Gong, C., Voigt, O., Melnyk, I., Keller, S., Klenk, M., . . . Fath, P. (2015). Bifacial Multicrystalline Solar Cells with Efficiencies above 18% Prepared in an Industrial Production Environment. *31st European Photovoltaic Solar Energy Conference and Exhibition, Hamburg, Germany, September 14-18, 2015*. (pp. 355-358). Red Hook, NY: Curran Associates, Inc. doi:<https://doi.org/10.4229/EUPVSEC20152015-2BO.4.5>
- Tyagi, V. V., Rahim, N., Rahim, N. A., & Selvaraj, J. (2013). Progress in solar PV technology: Reserach and achievement. *Renewable and Sustainable Energy Reviews*, *20*, 443-461. doi:<https://doi.org/10.1016/j.rser.2012.09.028>
- Vandeput, N. (2019, July 5). *Forecasts KPI:s RMSE, MAE, MAPE & Bias*. Retrieved June 8, 2021, from [towardsdatascience.com: https://towardsdatascience.com/forecast-kpi-rmse-mae-mape-bias-cdc5703d242d](https://towardsdatascience.com/forecast-kpi-rmse-mae-mape-bias-cdc5703d242d)
- Vattenfall. (2021a). *Elnätspriser*. Retrieved April 13, 2021, from [vattenfalleldistribution.se: https://www.vattenfalleldistribution.se/foretag/el-till-verksamheten/elnaetspriser/](https://www.vattenfalleldistribution.se/foretag/el-till-verksamheten/elnaetspriser/)
- Vattenfall. (2021b). *Energiskatt på el för 2020 och 2021*. Retrieved April 13, 2021, from [vattenfall.se: https://www.vattenfall.se/foretag/elavtal/energiskatter/](https://www.vattenfall.se/foretag/elavtal/energiskatter/)
- Vattenfall. (2021c). *Prishistorik över Rörligt elpris*. Retrieved April 13, 2021, from [vattenfall.se: https://www.vattenfall.se/elavtal/elpriser/rorligt-elpris/prishistorik/](https://www.vattenfall.se/elavtal/elpriser/rorligt-elpris/prishistorik/)
- Vattenfall. (2021d). *Ersättning och avgifter för elproduktion*. Retrieved April 22, 2021, from [vattenfalleldistribution.se: https://www.vattenfalleldistribution.se/foretag/producera-el/ersattning-och-avgifter/](https://www.vattenfalleldistribution.se/foretag/producera-el/ersattning-och-avgifter/)
- Vännman, K., & Jonsson, A. (2020). *Matematisk Statistik*. Lund: Studentlitteratur AB.
- Wali, Q., Elumalai, N. K., Iqbal, Y., Uddin, A., & Jose, R. (2018). Tandem perovskite solar cells. *Renewable perovskite solar cells*, 89-110. doi:<https://doi.org/10.1016/j.rser.2018.01.005>
- Wang, D., Liang, S., He, T., Yu, Y., Schaaf, C., & Wang, Z. (2015b). Estimating daily mean land surface albedo from Modis data. *Journal of Geophysical Research: Atmospheres*, *120*(10), 4825-4841. doi:<https://doi.org/10.1002/2015JD023178>
- Wang, S., Wilkie, O., Lam, J., Steeman, R., Zhang, W., Khoo, K. S., . . . Rostan, H. (2015a). Bifacial Photovoltaic Systems Energy Yield Modelling. *Energy Procedia*, *77*, 428-433. doi:<https://doi.org/10.1016/j.egypro.2015.07.060>
- Wang, Z., Zeng, X., & Barlage, M. (2007). Moderate Resolution Imaging Spectroradiometer bidirectional reflectance distribution function–based albedo parameterization for weather and climate models. *Journal of Geophysical Research*, *112*. doi:<https://doi.org/10.1029/2005JD006736>

- Wei, Q., Zhang, S., Yu, S., Lu, S., Lian, W., & Ni, Z. (2017). High efficiency n-PERT solar cells by B/P co-diffusion method. *7th International Conference on Silicon Photovoltaics* (pp. 700-705). Freiburg: Energy Procedia.
doi:<https://doi.org/10.1016/j.egypro.2017.09.345>
- Willmott, C. (1982). Some Comments on the Evaluation of Model Performance. *Bulletin of the American Meteorological Society*, *63*(11), 1309-1313.
doi:[https://doi.org/10.1175/1520-0477\(1982\)063<1309:SCOTEO>2.0.CO;2](https://doi.org/10.1175/1520-0477(1982)063<1309:SCOTEO>2.0.CO;2)
- Woodhouse, M., Marion, B., Huang, S., Feldman, D., Smith, B., & Margolis, R. (2019). Considerations for Utilizing Bifacial Photovoltaic Technologies Based Upon Their Impact to Project Financial Metrics. *Proceedings 2019 Bifacial PV Workshop*. Amsterdam. Unpublished manuscript.
- Yang, F., Mitchell, K., Hou, Y. T., Dai, Y., Zeng, X., Wang, Z., & Liang, X. Z. (2008). Dependence of Land Surface Albedo on Solar Zenith Angle: Observations and Model Parameterization. *Journal of Applied Meteorology and Climatology*, *47*(11), 2963-2982. doi:<https://doi.org/10.1175/2008JAMC1843.1>
- Zhang, C., Shen, H., Sun, L., Yang, J., Wu, S., & Lu, Z. (2020). Bifacial p-Type PERC Solar Cell with Efficiency over 22% Using Laser Doped Selective Emitter. *Energies*, *13*(6), 1388. doi:<https://doi.org/10.3390/en13061388>
- Zhang, T. (2017a, August 14). *What's a good value for kWh/kWp? An overview of specific yield*. Retrieved May 24, 2021, from Solar Power World:
<https://www.solarpowerworldonline.com/2017/08/specific-yield-overview/>
- Zhang, Y. F., Wang, X., Pan, Y. X., & Hu, R. (2012). Diurnal and seasonal variations of surface albedo in a spring wheat field of arid lands of Northwestern China. *International Journal of Biometeorology*, *57*(1), 67-73. doi:<https://doi.org/10.1007/s00484-012-0534-x>
- Zhang, Y., Campana, P. E., Lundblad, A., Wang, L., & Yan, J. (2017b). The influence of Photovoltaic Models and Battery Models in System Simulation and Optimization. *Energy Procedia*, *105*, 1184-1191. doi:<https://doi.org/10.1016/j.egypro.2017.03.409>



MÄLARDALEN UNIVERSITY
SWEDEN

P.O. Box 883, SE-721 23 Västerås, Sweden **Phone: +46 21 101 300**
P.O. Box 325, SE-631 05 Eskilstuna, Sweden **Phone: +46 16 153 600**
E-mail: info@mdh.se Webb: www.mdh.se